Thermo-rheologically complex polymers: multiaxial constitutive modeling, numerical implementation and experimental validation

Paolo Iaccarino, Ernesto Di Maio, Andrei Constantinescu, Ferdinando Auricchio

Highlights

Thermo-rheologically complex polymers: multiaxial constitutive modeling, numerical implementation and experimental validation

Paolo Iaccarino, Ernesto Di Maio, Andrei Constantinescu, Ferdinando Auricchio

- We report the development, implementation and validation of a constitutive model to describe the viscoelastic behavior of thermo-rheologically complex polymers
- Calorimetry analysis and tensile, shear and torsion frequency sweep experiments are performed on polypropylene and compared with literature data
- A multiaxial linear viscoelastic constitutive model for the behavior of thermo-rheologically complex polymers is reported in the time and frequency domain
- A regularization step has been implemented in the identification procedure proposed by Jalocha et al. (2015) to face with a large set of experimental data
- Frequency-temperature superposition principle has been applied on the experimental data by means of the horizontal and vertical shift functions, which appears explicitly in the constitutive model
- The constitutive model has been calibrated in the frequency domain and experimentally validated in the time domain by means of stress-relaxation and creep experiments

Thermo-rheologically complex polymers: multiaxial constitutive modeling, numerical implementation and experimental validation

Paolo Iaccarino[a,b,c], Ernesto Di Maio[b,c], Andrei Constantinescu[d,*] and Ferdinando Auricchio[e]

[a]Scuola Superiore Meridionale, Largo San Marcellino 10, Naples, 80138, Italy
[b]Dipartimento di Ingegneria Chimica, dei Materiali e della Produzione Industriale, University of Naples Federico II, P.le Tecchio 80, Naples, 80125, Italy
[c]foamlab, University of Naples Federico II, P.le Tecchio 80, Naples, 80125, Italy
[d]Laboratoire de Mécanique des Solides, CNRS, École Polytechnique, Institut Polytechnique de Paris, Palaiseau, 91128, France
[e]Dipartimento di Ingegneria Civile e Architettura, University of Pavia, Via Ferrata 3, Pavia, 27100, Italy

ARTICLE INFO

Keywords:
thermo-rheologically complex polymers
constitutive modeling
time-frequency superposition
parameter identification
experimental validation

ABSTRACT

We propose a simple multiaxial linear viscoelastic constitutive model to describe the behavior of thermo-rheologically complex polymers in both the time and frequency domains. The numerical implementation is discussed along with the parameter identification procedure. In particular, we propose a modification of the parameter identification procedure proposed by Jalocha et al. (2015) introducing a regularization step, enabling robust handling of large experimental datasets. We perform an extensive experimental investigation, including calorimetry analysis, as well as tensile, shear, and torsion frequency sweep, creep, and stress-relaxation experiments, and results are benchmarked against existing literature. The frequency-temperature superposition principle is applied to the experimental data using horizontal and vertical shift functions, explicitly integrated into the constitutive model framework. The calibration of the constitutive model is performed in the frequency domain, while the validation is performed in the time domain, demonstrating the accuracy and reliability of the model in multiple experimental domains. Finally, model predictions are reported in the frequency domain for different temperatures.

1. Introduction

The macro-scale thermo-mechanical behavior of polymers strongly depends on the experimentally investigated loading rate and temperature, reflecting at the macro-scale the structural transitions[1] occurring at the micro-scale [**ding2006breakdown**, **roland2005supercooled**, **kolsky1949investigation**, **klompen1999nonlinear**]. The time dependence of structural transitions can be described by evolutionary time-rate equations, often based on the introduction of simple mechanical models constructed from a discrete number of springs and dashpots [**anand2020continuum**]: from these simple mechanical models, one can retrieve a discrete spectrum of time-scales, being able to describe the loading rate dependence of polymers [**ngai1995identification**].

Since polymers are materials composed of macromolecules [**IUPAC+P04735+2019**], i.e., very large molecules with molecular weights ranging from a few thousands to millions of grams/mole, from a physical point of view each time-scale would represent a characteristic *relaxation time* of the constituent macromolecules [**rouse1953theory**]. At the micro-scale, macromolecules require a specific amount of time to relax in response to a given macroscopic deformation: this is, indeed, the relaxation time. If the temperature changes, such time changes accordingly: as temperature increases, macromolecules move and adjust more rapidly, whereas at lower temperatures they require more time to reorganize. For such a reason, relaxation times must have an inherent temperature dependence [**williams1955temperature**, **schmidtke2015temperature**].

*Corresponding author
thumbnails/cas-email.jpeg
paolo.iaccarino@unina.it (P. Iaccarino); edimaio@unina.it (E. Di Maio); andrei.constantinescu@polytechnique.edu (A. Constantinescu); ferdinando.auricchio@unipv.it (F. Auricchio)
ORCID(s): 0000-0002-1935-1324 (P. Iaccarino); 0000-0002-3276-174X (E. Di Maio); 0000-0003-4702-4256 (A. Constantinescu); 0000-0002-3735-2400 (F. Auricchio)

[1]Structural transitions in polymeric materials are accompanied by important changes in physical properties at the macro-scale, but there are no changes in the configuration at the micro-scale. The phases in a structural transition are distinguished by their *dynamic*, rather than static, properties.

Within the general class of polymers, the so-called thermo-rheologically simple polymers, by definition, show the same temperature dependence for all relaxation times, leading to equal acceleration (or deceleration) for all relaxation times by increasing (or decreasing) temperature [**rouse1953theory**, **van1998time**, **klompen1999nonlinear**]; examples of thermo-rheologically simple polymers can be single phase, amorphous homopolymers, and random copolymers [**emri2005rheology**]. Therefore, for thermo-rheologically simple polymers, there exists an equivalence relationship between the temperature and the time scale, and there exists a time-temperature *horizontal shift function* that defines the equivalence itself, which essentially describes the temperature dependence of the relaxation times [**hufferd1980thermoviscoelastic**, **van1998time**] and which has a very strong theoretical framework [**emri2005rheology**, **mccrum1964measurement**, **fesko1974time**, **mccrum1984kinetics**, **rusch1968time**, **rusch1968relaxational**, **bueche1954viscoelastic**, **dealy2009time**].

The existence of such a horizontal shift function is the key feature of the well-known Time-Temperature Superposition (TTS) principle. To clarify such a principle, we can consider a typical experimental campaign in which we perform stress relaxation or creep experiments in the same time window at different, but constant, temperatures. The outcome of the experimental campaign will be a set of isothermal relaxation functions or creep compliancies (generally referred to as viscoelastic functions). The TTS states that such isothermal viscoelastic functions can be horizontally shifted along the time axis through the time-temperature horizontal shift function, allowing them to collapse into a *mastercurve*, which corresponds to the behavior of the material at a given *reference temperature* [**arai1986temperature**, **van1998time**].

The same horizontal shift function is also the key feature of the Frequency-Temperature Superposition (FTS) principle, which is the TTS principle but in the frequency domain. In fact, we can consider an experimental campaign in which we perform frequency sweep experiments[2] in the same frequency window at different, but constant, temperatures. The outcome of the experimental campaign will be a set of isothermal moduli functions. The FTS principle states that such isothermal moduli functions can be horizontally shifted along the frequency axis through the time-temperature horizontal shift function, allowing them to collapse into a mastercurve which corresponds to the behavior of the material in the frequency domain at a given reference temperature [**hernandez2017thermorheologically**].

If the polymer is thermo-rheologically simple, such mastercurves are of vital importance in engineering, since they allow for a reliable extrapolation of the data of the material behavior at a given temperature at very short or very long time-scales (which can be inaccessible to standard experimental apparatus) [**oseli2016time**, **boussabnia2023validation**].

It should be emphasized that the formation of such mastercurves through horizontal shift of isothermal data is a necessary but not sufficient condition to classify a material as thermo-rheologically simple [**harper1985characterization**]; accordingly, if the TTS (or the FTS) principle is not applicable, the material cannot be considered thermo-rheologically simple.

In view of the framework introduced, in the present work we refer to a *thermo-rheologically complex polymer* as any polymeric material whose isothermal data cannot collapse into mastercurves solely by a horizontal shift. In thermo-rheologically complex polymers, different phases coexist, each exhibiting at the micro-scale its own time-temperature dependence of relaxation times: at the macro-scale, such different time-temperature dependencies combine and cannot be simply decoupled, both theoretically and experimentally. Furthermore, due to the interaction between different phases, the viscoelastic functions of a single phase may exhibit an additional temperature dependence, superimposed on the inherent temperature dependence of relaxation times [**emri2005rheology**]. Examples of thermo-rheologically complex polymers are block and graft copolymers, blends, viscoelastic composites [**brinson1991thermorheologically**], filled-reinforced elastomers [**garcia2023carbon**], and semi-crystalline polymers [**van1998time**, **emri2005rheology**].

Specifically regarding the case of semi-crystalline polymers, experimental calorimetry data reveals the presence of two structural transitions: more precisely, the first structural transition can be related to the glass transition[3] of the *mobile* amorphous phase, while the other can be related to the glass transition of the *rigid* amorphous phase [**beck1963glass**, **boyer1973apparent**, **grebowicz1984thermal**, **schawe2015analysis**]. The mobile amorphous phase consists of macromolecules which are *not* constrained by the surrounding crystals, while, on the contrary, the rigid

[2] A frequency sweep experiment is a type of experiment used to study the viscoelastic properties of materials by applying an oscillatory (sinusoidal) strain or stress at different frequencies.

[3] The most important structural transition in polymers is the glass transition, which is a structural transition between a glassy and a rubbery states of the amorphous part of the material. Both glassy and rubbery states lack long-range order (that is, no translational symmetry) and, as any other structural transition, they are distinguished by their dynamic properties. This means that the glass transition, as any other structural transition in polymers (such as structural transitions that can be related to end-group, side-group, or chain segments of macromolecules), presents a characteristic time-scale. More details on the glass transition can be found in the work of Shen and Eisenberg [**shen1967glass**].

amorphous phase constists of macromolecules which are mechanically constrained by the surrounding crystals. The presence of the glass transition of the rigid amorphous phase might be considered as the reason for the thermo-rheologically complex behavior of the material: such a transition has a direct effect on the macroscopic stiffness by adding an additional temperature dependence to viscoelastic functions, since it directly affects the network of crystals at the micro-scale, as in the case of filled rubbers [**kluppel2008evaluation**, **fritzsche2010structural**, **garcia2023carbon**].

For some thermo-rheologically complex polymers, it has been observed that mastercurves can still be constructed introducing a *vertical shift function* along with the horizontal shift function, apparently maintaining the validity of the TTS (or FTS) principle [**harper1985characterization**, **klompen1999nonlinear**]. A clear explanation and visualization of such a construction can be found in the work of Rouleau et al. [**rouleau2013application**].

However, to date, vertical shift functions have been largely empirical with very little theoretical validity [**emri2005rheology**, **mccrum1964measurement**, **fesko1974time**, **mccrum1984kinetics**, **rusch1968time**, **rusch1968relaxatio** **bueche1954viscoelastic**, **dealy2009time**]. In fact, in the literature it has been reported that aging, heat treatments, and crystallinity can also affect the vertical shift function and that when a vertical shift function is required, the horizontal shift function has an exponential dependence on the temperature [**williams1955temperature**, **kyu1976dynamic**]. Therefore, due to the lack of a strong theoretical background in contrast to what was the case for the horizontal shift function, whenever the vertical shift function is required, the resulting mastercurves are typically not used for the extrapolation of the data to estimate the response far from the experimental window [**landel1993mechanical**].

Such an intrinsic complexity of thermo-rheologically complex polymers and the fact that they are widely used in engineering applications have driven the development of various models and approaches aimed at better understanding their constitutive behavior, in order to predict their short and long term macro-scale thermo-mechanical behavior. Fesko and Tschoegl proposed a constitutive model based on the additivity of creep responses for two-phase materials [**fesko1974time**]. Such a model was studied in detail by Caruthers and Cohen [**caruthers1980consequences**] and extended in a further work by Kaplan and Tschoegl [**kaplan1974time**], but it should be used when the behavior of both phases is already known [**caruthers1980consequences**, **kaplan1974time**]. Brinson and Knauss proposed to model the thermo-rheologically complex behavior of a viscoelastic multi-phase material by means of the correspondence principle[4], but, as in the case of Kaplan and Tschoegl, the properties of the single phases of the composite should be known *a priori* to obtain reasonable results [**brinson1991thermorheologically**]. Following a different approach based on fractional calculus, Lenarda and Paggi developed a computational framework for thermo-rheologically complex polymers for the simulation of coupled thermo-mechanical problems [**lenarda2022computational**, **dusane2023computational**]. Harper and Weitsman introduced the most general constitutive equation for thermo-rheologically complex polymers, which can account for a vertical shift function [**weitsman1982thermoviscoelastic**, **harper1985characterization**]. In the theoretical framework proposed by Harper and Weitsman, Sadkin and Aboudi modeled the behavior of viscoelastic composites with a thermo-rheologically complex matrix [**sadkin1989viscoelastic**], while Muliana and Khan developed a nonlinear model for thermo-rheologically complex materials for small deformations and uncoupled thermo-mechanical problems [**muliana2008time**].

However, all existing models for thermo-rheologically complex polymers have been formulated in the time domain, whereas many applications, such as in vibration and damping, require material behavior to be expressed in the frequency domain [**sperling1990sound**]. Furthermore, the conversion between time and frequency domains is crucial both for practical use and for ensuring consistency across the domains: cross-validation between these domains becomes essential when experimental data are available in only one of them.

With such a background, the aim of the present work is to define viscoelastic multiaxial constitutive laws for thermo-rheologically complex polymers both in the time and frequency domains, as well as to include in the modeling the concept of vertical shift function, based on the pioneering work of Harper and Weitsman [**harper1985characterization**]. Once the model is defined, we describe the numerical implementation of the proposed model and the identification procedure of the model parameters. In particular, we use a recently introduced identification procedure [**jalocha2015revisiting**] modified by introducing a Tikhonov regularization step, so that it is now possible to deal with a large set of real experimental data. To validate both the model formulation and the implementation procedure, we planned an extensive experimental investigation on polypropylene (PP), a semi-crystalline polymer, which is used

[4]The correspondence principle between linear viscoelasticity and linear elasticity, or, simply, *the correspondence principle*, states that if for a given boundary-value problem the solution is known for a linear elastic material, then the same boundary-value problem for a linear viscoelastic material has a solution similar in form to the elastic solution, but in a Laplace transform space. More details and applications can be found in the book of Anand and Govindjee [**anand2020continuum**].

test type	l [mm]	w [mm]	t [mm]
tensile frequency sweep	$30^{\pm 1.5}$	$10^{\pm 0.5}$	$1^{\pm 0.1}$
shear frequency sweep	$40^{\pm 1.5}$	$15^{\pm 0.5}$	$0.5^{\pm 0.07}$
torsion frequency sweep	$30^{\pm 1.5}$	$10^{\pm 0.5}$	$2^{\pm 0.2}$
tensile stress-relaxation	$30^{\pm 1.5}$	$9^{\pm 0.5}$	$1^{\pm 0.1}$
tensile creep	$30^{\pm 1.5}$	$9^{\pm 0.5}$	$1^{\pm 0.1}$

Table 1
Dimensions of the prismatic samples for each type of test.

in a wide range of engineering applications [**maddah2016polypropylene**]. We perform (i) calorimetric tests and (ii) multiple frequency sweep tests under different load conditions, in particular in tensile, shear and torsion. For any of the load conditions, we build the mastercurves in the frequency domain using the FTS principle. We calibrate the model in the frequency domain and validate it in the time domain. To conclude, we show predictions of the model at different temperatures in the frequency domain.

The outline of the present work is the following: in section Materials, we describe the material used during experimental investigation and the samples production; in section Methods, we describe the adopted experimental methods, the proposed constitutive modeling, and the corresponding numerical discretization; in section Results, we show both the experimental and the numerical results; in section Conclusion we summarize the results and comment on the future perspectives of the present research; in Appendix, we share further details about the tensor notation, the numerical implementation, and additional experimental data from the literature to support our findings.

2. Materials

Polypropylene (PP) is provided by Sinopec Zhenhai Refining & Chemical Company (Zhejiang Province, China) in the form of beads (the technical code is E02ES). PP samples for testing are cut from PP sheets that are produced from PP beads using a compression molding machine (model P300P, Collin Gmbh, Ebersberg, Germany) and according to the following protocol: a) the mold is preheated to 200 °C, then the pellets are placed on the flat press table for 2 min without imposing any pressure; b) the pressure is increased up to 5 bar in 1 min, then to 10 bar in 1 min, and to 20 bar in 1 min; c) after cooling the plates (to 25 °C), we extract the PP sheet.

The samples for the DSC tests are cylindrical, with a diameter of $5^{\pm 0.1}$ mm and a height of $0.5^{\pm 0.08}$ mm. The average mass of such samples is $6.5^{\pm 0.5}$ mg. The samples for all the Dynamical Mechanical Anaysis (DMA) and rheometer tests are prismatic with dimensions reported in Table 1, where l is the length, w is the width and t is the thickness.

3. Methods

The thermal properties of PP are investigated using Differential Scanning Calorimetry (DSC) (Model Q2000, TA Instruments, New Castle, DE 19720). From DSC tests we obtain the heat flow as a function of the temperature, from which the specific heat, C_p, can be computed as follows:

$$C_p = \frac{\text{heat flow}}{mrM_M} \ , \tag{1}$$

where m is the mass of the sample, r is the scanning rate and M_M is the molecular weight of the repetitive unit of the polymer. We performed DSC tests with a scanning rate $r = 20$ °C/min and a temperature ranging from 10 to 180 °C. In the case of polypropylene, $M_M = 42.08$ g/mol. Each test is repeated three times to ensure the reliability of the result.

Tensile, shear, and torsion frequency sweep tests are performed at different temperatures. Tensile and shear frequency sweep tests are performed using a Dynamic Mechanical Analyzer (DMA) (DMA +1000, ACOEM Metravib, Limonest, France SAS) over a linear frequency range of 1 to 100 Hz (experimental setup in Figure 1(a) and (b), respectively). Torsion frequency sweep tests are performed using a rheometer (ARES, TA Instruments, USA) in an angular frequency range of 1 to 100 rad/s (experimental setup in Figure 1(c)). All tests are performed in strain control mode. We impose a dynamic strain of 0.1%, with $d_{\text{stat}}/d_{\text{dyn}} = 1.1$, where d_{stat} and d_{dyn} are the static and dynamic displacement (in the load direction) of the crosshead. To fix the sample, a dynamometric screwdriver at 1.3 N·m was

used. All tests are repeated two times. The error of the experimental data is of the order of 1.5% of the absolute value, as from DMA specification in the range of linear frequencies at which experiments are performed.

Stress relaxation and creep tests are performed in a tensile setting using DMA at $T = 30°\text{C}$. In the stress-relaxation test, we impose a static strain $\epsilon_0 = 0.1\%$. The time to reach a stable value of the static strain is about 20 s. In the creep test, we impose a static stress $\sigma_0 = 1.2 \times 10^6$ Pa. The time to reach a stable value of the static stress is about 0.5 s, and this is expected since the DMA hardware is force controlled.

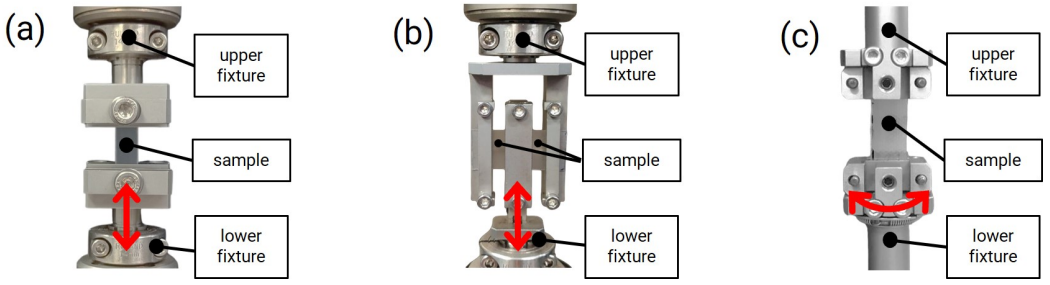

Figure 1: Experimental setups, where the red arrows represent the displacement direction of the lower fixture. (a) Tensile. (b) Shear. (c) Torsion.

4. Constitutive modeling

We consider an isotropic material that occupies a region $\Omega \subset \mathbb{R}^3$. We denote by $\boldsymbol{u}$ the displacement field and define the infinitesimal strain tensor as $\boldsymbol{\epsilon} = (\nabla \boldsymbol{u} + \nabla \boldsymbol{u}^T)/2$. We can split stress, $\boldsymbol{\sigma}$, and strain in volumetric and deviatoric components, that is:

$$\begin{cases} \boldsymbol{\sigma} &= p\mathbf{1} + \boldsymbol{s} \\ \boldsymbol{\epsilon} &= \dfrac{\theta}{3}\mathbf{1} + \boldsymbol{e} \end{cases} \quad \text{where} \quad \begin{cases} p &= \dfrac{1}{3}\mathrm{Tr}(\boldsymbol{\sigma}) \\ \theta &= \mathrm{Tr}(\boldsymbol{\epsilon}) \end{cases} \quad \text{and} \quad \begin{cases} \boldsymbol{s} = \mathbb{I}^{\mathrm{Ss}}_{\odot\mathrm{dev}}\, \boldsymbol{\sigma} \\ \boldsymbol{e} = \mathbb{I}^{\mathrm{Ss}}_{\odot\mathrm{dev}}\, \boldsymbol{\epsilon} \end{cases} . \tag{2}$$

For the notation on fourth-order tensors, the reader is referred to the Appendix. We assume an additive decomposition of the strain, that is, $\boldsymbol{\epsilon} = \boldsymbol{\epsilon}^e + \boldsymbol{\epsilon}^v$, where $\boldsymbol{\epsilon}^e$ is the elastic strain and $\boldsymbol{\epsilon}^v$ is the viscous (and hence, inelastic) strain, the latter considered as the internal variable. Consistently with Equation 2, we can split the elastic and viscous strains in volumetric and deviatoric components:

$$\begin{cases} \boldsymbol{\epsilon}^e = \dfrac{1}{3}\theta^e\mathbf{1} + \boldsymbol{e}^e \\ \boldsymbol{\epsilon}^v = \dfrac{1}{3}\theta^v\mathbf{1} + \boldsymbol{e}^v \end{cases} \quad \text{where} \quad \begin{cases} \boldsymbol{e} = \boldsymbol{e}^e + \boldsymbol{e}^v \\ \theta = \theta^e + \theta^v \end{cases} . \tag{3}$$

Following Anand and Govindjee [**anand2020continuum**], the viscoelastic behavior is said to be linear when viscoelastic functions, i.e., stress relaxation, creep and complex moduli functions, are independent of the magnitude of the applied strain or stress. In the present work, we use a generalized Maxwell model to describe the linear viscoelastic behavior of the PP; the formulation herein is also equivalent to that used by Zienkiewicz and Taylor [**zienkiewicz2005finite**] and by Holzapfel [**Holzapfel2000Visco**].

The linear viscoelastic material behaviour will be model using a Generalized Maxwell model. This model has been proven to be effective and robust for the representation of solid polymers, see for example [**xu2020new**, **gebrehiwot2022characterising**]. This permits a straightforward passage from the time domain to the frequency, and the relaxation tensor leads to the well-known *Prony series* [**soussou1970application**], which gives an easy numerical integration in predictor-corrector algorithms in finite element simulations [**simo2006computational**]. This passage leads to more complex formulae in the case of the generalized Kelvin-Voigt model [**d1988viscoelastic**]. Let us further remark that DMA experiments provide relaxation moduli, which naturaly brings the data interpretation to the more simpler relaxation times rather than to retardation times [**baumgaertel1989determination**].

We can hence write the generalized Maxwell model composed of N Maxwell branches in a time-continuous setting as

$$\begin{cases} p &= K_\infty \theta + \sum_j K_j(\theta - \theta_j^v) \\ \boldsymbol{s} &= 2G_\infty \boldsymbol{e} + 2\sum_j G_j \left(\boldsymbol{e} - \boldsymbol{e}_j^v\right) \end{cases} \quad \text{with} \quad \begin{cases} \dot{\theta}_j^v &= \dfrac{1}{\tau_j}\left(\theta - \theta_j^v\right) \\ \dot{\boldsymbol{e}}_j^v &= \dfrac{1}{\tau_j}\left(\boldsymbol{e} - \boldsymbol{e}_j^v\right) \end{cases} , \tag{4}$$

where $j = 1, ..., N$, with the conditions that $\lim_{t\to-\infty} \boldsymbol{e}_j^v = \boldsymbol{0}$ and $\lim_{t\to-\infty} \theta_j^v = 0$. In Equation 4, the index j refers to the j-th Maxwell branch (being τ_j its relaxation time), then: θ_j^v and $\boldsymbol{e}_j^v$ are the viscous volumetric and deviatoric strains; K_j and G_j are the bulk and shear relaxation moduli. The model is shown in 1D for the deviatoric component of the stress in Figure 2.

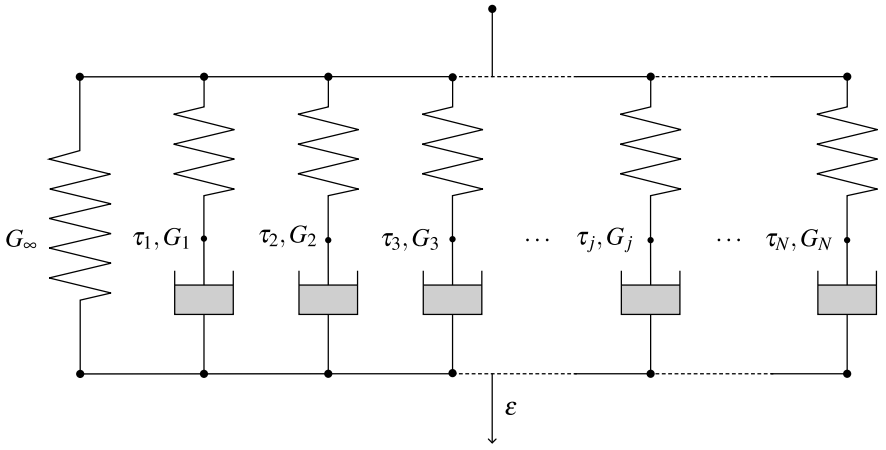

Figure 2: Generalized Maxwell model adopted herein, reported in 1D.

When the model in Equation 4 is subjected to a multiaxial stress relaxation test, i.e., at time $t = 0$ we impose a given step strain of magnitude $\boldsymbol{\epsilon} = \boldsymbol{\epsilon}_0$ which is held constant in time, the following solution is obtained:

$$\boldsymbol{\sigma}(t) = \mathbb{G}_r(t)\boldsymbol{\epsilon}_0 \ , \tag{5}$$

where $\mathbb{G}_r(t)$ is the fourth-order stress-relaxation tensor

$$\mathbb{G}_r(t) = K_r(t)\underset{\otimes}{\mathbb{I}} + 2G_r(t)\underset{\odot_{\text{dev}}}{\mathbb{I}^{\text{Ss}}} \ , \tag{6}$$

with

$$K_r(t) = K_\infty + \sum_j^N K_j \exp\left(-\frac{t}{\tau_j}\right) \quad \text{and} \quad G_r(t) = G_\infty + \sum_j^N G_j \exp\left(-\frac{t}{\tau_j}\right) \ . \tag{7}$$

In the field of rheology, these functional forms are also known as Prony series [**soussou1970application**], which are widely exploited for computational purposes in linear viscoelasticity due to their discrete nature [**sekmen2023curing**, **gouhier2024finite**].

Once we have obtained $\mathbb{G}_r(t)$, we can calculate the multiaxial stress response as a function of the (actual) time t for any given multiaxial strain history, $\boldsymbol{\epsilon}(t)$, as follows:

$$\boldsymbol{\sigma}(t) = \int_{0^-}^{t} \mathbb{G}_r\left(t - \tau\right) : \frac{\mathrm{d}\boldsymbol{\epsilon}(\tau)}{\mathrm{d}\tau}\mathrm{d}\tau \ , \tag{8}$$

where τ is the elapsed time, which is simply the time that has elapsed up to the actual instant t [**anand2020continuum**].

Equation 8 with the functional forms $K_r(t)$ and $G_r(t)$ represents the generalized Maxwell linear viscoelastic model in the time domain. Now that we have derived the model in the time domain, it would be beneficial to transform it into the frequency domain: in fact, many experimental studies in polymer mechanics, such as those involving DMA or rheometry, are typically conducted in the frequency domain.

In order to move towards the frequency domain, we first compute the Laplace transform, $\mathscr{L}[\cdot]$, of Equation 8:

$$\underbrace{\mathscr{L}[\boldsymbol{\sigma}(t)]}_{\hat{\boldsymbol{\sigma}}(s)} = \underbrace{s\mathscr{L}[\mathbb{G}_r(t)]}_{\hat{\mathbb{G}}_r(s)} : \underbrace{\mathscr{L}[\boldsymbol{\epsilon}(t)]}_{\hat{\boldsymbol{\epsilon}}(s)} \ , \tag{9}$$

and using the properties of the Laplace transform (see Appendix) we obtain

$$\hat{\boldsymbol{\sigma}}(s) = \hat{\mathbb{G}}_r(s) : \hat{\boldsymbol{\epsilon}}(s) \ , \tag{10}$$

where $s = a + \mathrm{i}\omega \in \mathbb{C}$, and

$$\hat{\mathbb{G}}_r(s) = \hat{K}_r(s)\mathbb{I}_{\otimes} + 2\hat{G}_r(s)\mathbb{I}^{\mathrm{Ss}}_{\odot_{\mathrm{dev}}} \ , \tag{11}$$

with

$$\hat{K}_r(s) = s\mathscr{L}[K_r(t)] = K_\infty + \sum_j^N K_j \frac{s\tau_j}{1+\tau_j s} \quad \text{and} \quad \hat{G}_r(s) = s\mathscr{L}[G_r(t)] = G_\infty + \sum_j^N G_j \frac{s\tau_j}{1+\tau_j s} \ . \tag{12}$$

Equation 10 with the functional forms $\hat{K}_r(s)$ and $\hat{G}_r(s)$ represents the generalized Maxwell linear viscoelastic model in the the complex frequency domain, also known as the s domain: in fact, the Laplace transform decompose the original time domain function into exponential of the form $\exp(st)$ (see again the Appendix).

However, in a DMA experiment, the material is probed in the frequency domain, in which a sinusoidal strain (or stress) signal with a constant amplitude is applied and in which there is no decay (or growth) of the stress or strain (i.e., there is no the real part of s, since the initial transient part of the stress or strain signal is neglected in the DMA measurement); accordingly, it is more convenient to decompose the original time-domain model in exponential of the form $\exp(\mathrm{i}\omega t)$, that is, by evaluating the Laplace transform on its imaginary axis, where, from a physical point of view, no dissipation or damping of the stress or strain signal is considered.

When we evaluate the Laplace transform on the imaginary axis by imposing $s = \mathrm{i}\omega$, we obtain the Fourier transform, $\mathscr{F}[\cdot]$, of the original time domain model, expressed in the frequency (ω) domain. Hence, from Equation 12, we obtain:

$$\hat{K}_r(\omega) = K_\infty + \sum_j^N K_j \frac{\mathrm{i}\omega\tau_j}{1+\mathrm{i}\omega\tau_j} \quad \text{and} \quad \hat{G}_r(\omega) = G_\infty + \sum_j^N G_j \frac{\mathrm{i}\omega\tau_j}{1+\mathrm{i}\omega\tau_j} \ . \tag{13}$$

Now, the fourth order stress-relaxation tensor in the frequency domain, $\hat{\mathbb{G}}_r(\omega)$, becomes

$$\hat{\mathbb{G}}_r(\omega) = \hat{K}_r(\omega)\mathbb{I}_{\otimes} + 2\hat{G}_r(\omega)\mathbb{I}^{\mathrm{Ss}}_{\odot_{\mathrm{dev}}} \ , \tag{14}$$

and can be rewritten as

$$\hat{\mathbb{G}}_r(\omega) = 2\mathfrak{R}\{\hat{\mathbb{G}}_r(\omega)\} + \mathrm{i}\mathfrak{I}\{\hat{\mathbb{G}}_r(\omega)\} \ , \tag{15}$$

where

$$\begin{aligned}\mathfrak{R}\{\hat{\mathbb{G}}_r(\omega)\} &= 2\left(G_\infty + \sum_j^N G_j \frac{(\omega\tau_j)^2}{1+(\omega\tau_j)^2}\right) \mathbb{I}^{\mathrm{Ss}}_{\ominus_{\mathrm{dev}}} + \left(K_\infty + \sum_j^N K_j \frac{(\omega\tau_j)^2}{1+(\omega\tau_j)^2}\right) \mathbb{I}_{\otimes} \\ \mathfrak{I}\{\hat{\mathbb{G}}_r(\omega)\} &= 2\left(\sum_j^N G_j \frac{\omega\tau_j}{1+(\omega\tau_j)^2}\right) \mathbb{I}^{\mathrm{Ss}}_{\ominus_{\mathrm{dev}}} + \left(\sum_j^N K_j \frac{\omega\tau_j}{1+(\omega\tau_j)^2}\right) \mathbb{I}_{\otimes} \ .\end{aligned} \tag{16}$$

Equations 15 and 16 represent the generalized Maxwell model in the frequency domain. It can be observed that if $\omega \to \infty$, then $\mathfrak{I}\{\hat{\mathbb{G}}_r(\omega)\} \to \mathbb{O}$; in such a case, only $\mathfrak{R}\{\hat{\mathbb{G}}_r(\omega)\}$ exists, and the linear viscoelastic material behaves as a purely elastic material with $G_r|_{\omega\to\infty} = G_\infty + \sum_j^N G_j$ and $K_r|_{\omega\to\infty} = K_\infty + \sum_j^N K_j$. Again, if $\omega \to 0$, then $\mathfrak{I}\{\hat{\mathbb{G}}_r(\omega)\} \to \mathbb{O}$ and the linear viscoelastic material behave as a purely elastic material with $G_r|_{\omega\to 0} = G_\infty$ and $K_r|_{\omega\to 0} = K_\infty$.

Thermo-rheologically simple polymers. Recalling that thermo-rheologically simple polymers show the same temperature dependence for all relaxation times and that such a dependence should be described by the horizontal shift function, we can now modify Equation 8 to introduce such a function.

Starting from Anand and Govindjee [**anand2020continuum**] and according to Harper and Weitsman [**harper1985characteri**] the multiaxial stress response as a function of the (actual) time t of a thermo-rheologically simple material subjected to a time-dependent temperature history can be written as

$$\boldsymbol{\sigma}(t) = \int_{0^-}^{t} \mathbb{G}_r\left(\xi(t) - \xi(\tau)\right) : \frac{\mathrm{d}\boldsymbol{\epsilon}(\tau)}{\mathrm{d}\tau}\mathrm{d}\tau \ , \tag{17}$$

where $\xi(\tau)$ is the *reduced time* and it is herein defined by:

$$\xi(\tau) = \int_0^{\tau} \frac{\mathrm{d}x}{a_T(T(x), T_{ref})} \ , \tag{18}$$

where $a_T(T(t), T_{ref})$ is the horizontal shift function, which depends on the temperature history $T(t)$ and the reference temperature, T_{ref}. T_{ref} is a fundamental ingredient in the model: we model the behavior of the material for $T(t)$ with respect to such a reference temperature, meaning that all the values t_j, K_j and G_j introduced in Equation 4 will be referred to the reference temperature, T_{ref}.

From Equation 18, it is possible to see that the horizontal shift function is introduced in the constitutive equation through reduced time. Such a reduced time is a longer or shorter time with respect to the actual time, depending on the actual temperature [**anand2020continuum**, **taylor1970thermomechanical**]. In particular, (i) if the actual temperature is equal to the reference temperature, the actual time coincides with the reduced time; (ii) if the actual temperature is higher than the reference temperature, the actual time is shorter than the reduced time; (iii) if the actual temperature is lower than the reference temperature, the actual time is longer than the reduced time.

Given the constitutive equation reported in Equation 17, we can check that the material behavior is shifted towards the time axis when one wants to construct an experimental mastercurve when applying the TTS principle. Since to apply such a principle the temperature is kept constant and equal to T_n for each isothermal temperature step, Equation 18 becomes

$$\xi(t) = \int_0^{t} \frac{ds}{a_T(T_n, T_{ref})} = \frac{t}{a_T(T_n, T_{ref})} \ . \tag{19}$$

and $G_r(t)$ and $K_r(t)$ become, for each step

$$
\begin{aligned}
G_r(t)|_{T_n}^{\mathrm{TS}} &= G_\infty + \sum_j^N G_j \exp\left(-\frac{t}{a_T(T_n, T_{ref})\tau_j}\right) \\
K_r(t)|_{T_n}^{\mathrm{TS}} &= K_\infty + \sum_j^N K_j \exp\left(-\frac{t}{a_T(T_n, T_{ref})\tau_j}\right) \quad .
\end{aligned}
\tag{20}
$$

Such a model is enough to describe thermo-rheologically simple polymers and hence to construct a mastercurve. In fact, $a_T(T_n, T_{ref})$ shifts the relaxation times along the time axis, as required.

Thermo-rheologically complex polymers. In the case of thermo-rheologically complex polymers, the horizontal shift function is not enough to take into account the complexity of the material, since mastercurves cannot be constructed by using only the horizontal shift function. We can assume that the thermo-rheological complexity can be described as an additional temperature dependence of the viscoelastic functions at the macro-scale, which is not related to the shift of relaxation times [**emri2005rheology**]. Such additional temperature dependence can be introduced through a vertical shift function, b_T, in Equation 20 that directly acts on the relaxation moduli.

Accordingly to what we have assumed for the horizontal shift function, we can assume that the vertical shift function depends only on the actual temperature and the reference temperature. In fact, if measurements are made in isothermal steps and under equilibrium conditions, we do not need other assumptions [**taylor1970thermomechanical**]. We can write the relaxation functions at a temperature step T_n, as follows:

$$
\begin{aligned}
G_r(t)|_{T_n}^{\mathrm{TC}} &= b_T(T_n, T_{ref}) \left[G_\infty + \sum_j^N G_j \exp\left(-\frac{t}{a_T(T_n, T_{ref})\tau_j}\right) \right] \\
K_r(t)|_{T_n}^{\mathrm{TC}} &= b_T(T_n, T_{ref}) \left[K_\infty + \sum_j^N K_j \exp\left(-\frac{t}{a_T(T_n, T_{ref})\tau_j}\right) \right] \quad .
\end{aligned}
\tag{21}
$$

As stated in the introduction, such an equation is similar with the 1D model proposed in the work of Harper and Weitsman for the creep of thermo-rheologically complex polymers [**harper1985characterization**]. Note that the relaxation times and moduli refer to the reference temperature.

Since the reference temperature is a constant value, to simplify the notation, from now on we will write $a_{T_n} = a_T(T_n, T_{ref})$ and $b_{T_n} = b_T(T_n, T_{ref})$. We now move towards the frequency domain, obtaining:

$$
\begin{aligned}
\hat{G}_r(\omega)|_{T_n}^{\mathrm{TC}} &= 2\mathrm{i}\omega\mathscr{F}[G_r(t)|_{T_n}^{\mathrm{TC}}] = 2b_{T_n}\left[G_\infty + \sum_j^N G_j \frac{\mathrm{i}\omega a_{T_n}\tau_j}{1 + \mathrm{i}\omega a_{T_n}\tau_j} \right] \\
\hat{K}_r(\omega)|_{T_n}^{\mathrm{TC}} &= \mathrm{i}\omega\mathscr{F}[K_r(t)|_{T_n}^{\mathrm{TC}}] = b_{T_n}\left[K_\infty + \sum_j^N K_j \frac{\mathrm{i}\omega a_{T_n}\tau_j}{1 + \mathrm{i}\omega a_{T_n}\tau_j} \right] \quad .
\end{aligned}
\tag{22}
$$

Now, the fourth order stress-relaxation tensor at a temperature T_n for a thermo-rheologically complex polymer in the frequency domain, $\hat{\mathbb{G}}_r|_{T_n}^{\mathrm{TC}}(\omega)$, become

$$
\hat{\mathbb{G}}_r|_{T_n}^{\mathrm{TC}}(\omega) = \hat{G}_r(\omega)|_{T_n}^{\mathrm{TC}} \mathbb{I}_{\odot_{\mathrm{dev}}}^{\mathrm{Ss}} + \hat{K}_r(\omega)|_{T_n}^{\mathrm{TC}} \mathbb{I}_{\otimes}^{\mathrm{Ss}} \quad ,
\tag{23}
$$

and can be rewritten as

$$
\hat{\mathbb{G}}_r|_{T_n}^{\mathrm{TC}}(\omega) = \mathfrak{R}\{\hat{\mathbb{G}}_r|_{T_n}^{\mathrm{TC}}(\omega)\} + \mathrm{i}\mathfrak{I}\{\hat{\mathbb{G}}_r|_{T_n}^{\mathrm{TC}}(\omega)\} \quad ,
\tag{24}
$$

where

$$\begin{aligned}\Re\{\hat{\mathbb{G}}_r|^{\mathrm{TC}}_{T_n}(\omega)\} &= b_{T_n}\left[2\left(G_\infty+\sum_j^N G_j\frac{(a_{T_n}\omega\tau_j)^2}{1+(a_{T_n}\omega\tau_j)^2}\right)\mathbb{I}^{\mathrm{Ss}}_{\odot_{\mathrm{dev}}}+\left(K_\infty+\sum_j^N K_j\frac{(a_{T_n}\omega\tau_j)^2}{1+(a_{T_n}\omega\tau_j)^2}\right)\mathbb{I}_{\otimes}\right]\\ \Im\{\hat{\mathbb{G}}_r|^{\mathrm{TC}}_{T_n}(\omega)\} &= b_{T_n}\left[2\left(\sum_j^N G_j\frac{a_{T_n}\omega\tau_j}{1+(a_{T_n}\omega\tau_j)^2}\right)\mathbb{I}^{\mathrm{Ss}}_{\odot_{\mathrm{dev}}}+\left(\sum_j^N K_j\frac{a_{T_n}\omega\tau_j}{1+(a_{T_n}\omega\tau_j)^2}\right)\mathbb{I}_{\otimes}\right]\quad .\end{aligned}\tag{25}$$

The equations derived are in accordance, for example, with Van Gurp and Palmen [**van1998time**].

Numerical discretization. To derive the discretization procedure, we consider a strain-driven process. Since the experiments are isothermal with different temperature, we also assume the temperature constant and equal to T_n, and hence $a_T = a_{T_n}$ and $b_T = b_{T_n}$. We use the Backward Euler formula to integrate the evolution equations of the internal variables, and we denote as $\Delta t = t_{k+1} - t_k$ the time step. If we write the quantities evaluated at t_k with the subscript k and the quantities evaluated at t_{k+1} with no subscript, we obtain the following discrete-time model:

$$\begin{cases} p &= b_{T_n}K_\infty\theta + b_{T_n}\sum_j K_j\left(\theta-\theta^v_j\right)\\ \boldsymbol{s} &= 2b_{T_n}G_\infty\boldsymbol{e}+2b_{T_n}\sum_j G_j\left(\boldsymbol{e}-\boldsymbol{e}^v_j\right)\end{cases}\quad\text{with}\quad\begin{cases}\theta^v_j &= \alpha_j\left[\theta^v_{j_k}+\beta_j\theta\right]\\ \boldsymbol{e}^v_j &= \alpha_j\left[\boldsymbol{e}^v_{j_k}+\beta_j\boldsymbol{e}\right]\end{cases},\tag{26}$$

with $j = 1, ..., N$, where

$$\alpha_j = \left[1+\frac{\Delta t}{a_{T_n}\tau_j}\right]^{-1}\quad\text{and}\quad\beta_j = \frac{\Delta t}{a_{T_n}\tau_j}\ ,\tag{27}$$

by imposing that $\boldsymbol{e}^v_{j_0} = \boldsymbol{0}$ and $\theta^v_{j_0} = 0\ \forall j$. After linearization of such a system of equations, the tangent matrix, $\mathbb{C}_{\mathrm{TG}}$, becomes:

$$\mathbb{C}_{\mathrm{TG}} = b_{T_n}\left(K_\infty+\sum_j K_j\alpha_j\right)\mathbb{I}_{\otimes}+2b_{T_n}\left(G_\infty+\sum_j G_j\alpha_j\right)\mathbb{I}^{\mathrm{Ss}}_{\odot_{\mathrm{dev}}}\ .\tag{28}$$

For the details on the numerical implementation, see Appendix A.

Identification procedure. Once the model is defined (Equation 24), the identification problem arises. In principle, the number of relaxation times, N, is unknown *a priori* [**jalocha2015revisiting**, **barrientos2019optimal**]. Many commercial algorithms (e.g., ABAQUS [**Abaq2024**]) use an equispaced distribution of relaxation times on the time logarithmic scale by *a priori* choosing N [**barrientos2019optimal**], eliminating one of the major unknowns of the identification problem. However, it has been reported that such a uniform predefined distribution of the relaxation times produces accurate fittings only under specific conditions [**barrientos2019optimal**], and it can also lead to non-physical results [**collet2013noise**].

Among the recent proposed criteria for the allocation of relaxation times [**tschoegl2012phenomenological**, **yue2021tri**, **marino2023automated**], Jalocha et al. [**jalocha2015revisiting**] developed an identification technique based on the mathematical result in complex analysis obtained by Krein and Nudelman [**krein1998interpolation**] and the application of such results to impact tests performed by Collet et al. [**collet2013noise**]. Such a method, named by the authors as the *KN + HW* method, involves two steps: *Step 1* is related to the identification of the number and location of the relaxation times (herein not chosen *a priori*); *Step 2* is related to the identification of the relaxation moduli values [**jalocha2015revisiting**]. Hence, based on the model of Equation 24 to apply the methodology to the mastercurves we herein formalize the *KN + HW* method proposed by Jalocha et al. [**jalocha2015revisiting**] for horizontally and vertically shifted data.

Step 1: identification of relaxation times. We consider a set of J DMA frequency sweep experiments performed within the same experimental window, defined as the range of frequencies covered in the experiment, and at a constant temperature T_j . If in the experimental window we acquire M frequency values, and hence we can write the experimental window as $\boldsymbol{\omega} = [\omega_1, ..., \omega_M]^T$, we obtain as experimental data the storage moduli $\boldsymbol{G'_j} = [G'_{j1}, ..., G'_{jM}]^T$ and the loss moduli $\boldsymbol{G''_j} = [G''_{j1}, ..., G''_{jM}]^T$. We recall that $\boldsymbol{G'_j}$ and $\boldsymbol{G''_j}$ are the (discrete and experimental) values of the real and imaginary parts of the stress-relaxation function in the frequency domain (Equation 16) at T_j. For each T_j, the complex modulus reads

$$\boldsymbol{G^*_j} = \boldsymbol{G'_j} + \mathrm{i}\boldsymbol{G''_j} \ . \tag{29}$$

Now, similarly to what has been done in the work of Jalocha et al. [**jalocha2015revisiting**], we can write the vector of shifted frequencies, $\tilde{\boldsymbol{\omega}}$, and the vector of shifted complex moduli, $\tilde{\boldsymbol{G}}^*$ (the vector which contains all the shifted moduli after the application of the Arai and Ferry procedure), with respect to the reference temperature T_{ref}, as

$$\tilde{\boldsymbol{\omega}} = \begin{bmatrix} a_{T_1}\boldsymbol{\omega} \\ \vdots \\ a_{T_J}\boldsymbol{\omega} \end{bmatrix} \in \mathbb{R}^{(M\cdot J)\times 1} \quad \text{and} \quad \tilde{\boldsymbol{G}}^* = \begin{bmatrix} b_{T_1}\boldsymbol{G^*_1} \\ \vdots \\ b_{T_J}\boldsymbol{G^*_J} \end{bmatrix} \in \mathbb{C}^{(M\cdot J)\times 1} \ . \tag{30}$$

The complex conjugate of $\tilde{\boldsymbol{G}}^*$ will be indicated as $\overline{\tilde{\boldsymbol{G}}^*}$. We define the two complex square matrices $\boldsymbol{M^1}, \boldsymbol{M^2} \in \mathbb{C}^{(M\cdot J)\times(M\cdot J)}$ [**jalocha2015revisiting**] as follows (by components):

$$M^1_{kl} = \mathrm{i}\frac{\overline{\tilde{G}^*_k} - \tilde{G}^*_l}{\tilde{\omega}_k + \tilde{\omega}_l} \quad \text{and} \quad M^2_{kl} = \frac{\dfrac{\overline{\tilde{G}^*_k}}{\tilde{\omega}_k} + \dfrac{\tilde{G}^*_l}{\tilde{\omega}_l}}{\tilde{\omega}_k + \tilde{\omega}_l} \ , \tag{31}$$

We now define as $\boldsymbol{v}$ and $\boldsymbol{w}$ the eigenvectors of the kernels of the matrices $\boldsymbol{M^1}$ and $\boldsymbol{M^2}$ respectively. They are associated with the eigenvalue 0, which implies that

$$\begin{aligned} \boldsymbol{v}\cdot\boldsymbol{M^1}\cdot\overline{\boldsymbol{v}} = 0 \\ \boldsymbol{w}\cdot\boldsymbol{M^2}\cdot\overline{\boldsymbol{w}} = 0 \ . \end{aligned} \tag{32}$$

The singular value decomposition can be used to find the eigenvectors of the kernels of $\boldsymbol{M^1}$ and $\boldsymbol{M^2}$. Alternatively, $\boldsymbol{v}$ and $\boldsymbol{w}$ are found solving iteratively Equation 32. Then, the relaxation times are $\tau_j = 1/s_j$, where s_j are the common zeros (in a numerical sense) of the rational functions $||f_1(s)||_2$ and $||f_2(s)||_2$ (derived from $\boldsymbol{M^1}$ and $\boldsymbol{M^2}$ respectively)

$$\left\|f_1(s)\right\|_2 = \left\| \sum_k^{M\times J} \frac{v_k}{(s - \mathrm{i}\tilde{\omega}_k)} \right\|_2 \quad \text{and} \quad \left\|f_2(s)\right\|_2 = \left\| \sum_k^{M\times J} \frac{w_k}{(s - \mathrm{i}\tilde{\omega}_k)} \right\|_2 \ , \tag{33}$$

where $\|\cdot\|_2$ is the L2-norm [**collet2013noise**, **jalocha2015revisiting**]. From the algorithm, N relaxation times are obtained. It should be emphasized that the relaxation times are computed at the reference temperature.

Step 2: identification of the relaxation moduli. Once the N relaxation times are identified by step 1, the N relaxation moduli have to be found. Having calculated the relaxation times in *Step 1* at the reference temperature, $\boldsymbol{G}$ will be computed at the reference temperature. Once again, the storage and loss moduli are rearranged as follows:

$$\tilde{\boldsymbol{G'}} = \begin{bmatrix} b_{T_1}\boldsymbol{G'_1} \\ \vdots \\ b_{T_J}\boldsymbol{G'_J} \end{bmatrix} \in \mathbb{R}^{(M\cdot J)\times 1} \quad \text{and} \quad \tilde{\boldsymbol{G''}} = \begin{bmatrix} b_{T_1}\boldsymbol{G''_1} \\ \vdots \\ b_{T_J}\boldsymbol{G''_J} \end{bmatrix} \in \mathbb{R}^{(M\cdot J)\times 1} \ . \tag{34}$$

Jalocha et al. [**jalocha2015revisiting**] proposed to solve in a least square sense the following systems of linear equations:

$$\tilde{\boldsymbol{G}}' = \boldsymbol{A}\boldsymbol{G} \quad \text{and} \quad \tilde{\boldsymbol{G}}'' = \boldsymbol{B}\boldsymbol{G} \ , \tag{35}$$

where $\boldsymbol{G} \in \mathbb{R}^{N\times 1}$ is the vector of relaxation moduli of the Prony series at reference temperature and the matrices $\boldsymbol{A}$ and $\boldsymbol{B}$ are defined as

$$\begin{aligned} \boldsymbol{A} &= (a_{ij}) \in \mathbb{R}^{(M\cdot J)\times N}, \quad a_{ij} = \frac{\tilde{\omega}_i^2\tau_j^2}{1+\tilde{\omega}_i^2\tau_j^2} \quad \text{with } i = 1...\ M;\ j = 1...\ N \\ \boldsymbol{B} &= (b_{ij}) \in \mathbb{R}^{(M\cdot J)\times N}, \quad b_{ij} = \frac{\tilde{\omega}_i\tau_j}{1+\tilde{\omega}_i^2\tau_j^2} \quad \text{with } i = 1...\ M;\ j = 1...\ N \ . \end{aligned} \tag{36}$$

Now, the vector $\boldsymbol{G}$ can be obtained by solving one of the two minimum problems:

$$\boldsymbol{G} = \underset{\boldsymbol{d}}{\operatorname{argmin}} \left\| \tilde{\boldsymbol{G}}' - \boldsymbol{A}\boldsymbol{d} \right\|_2^2 \quad \text{or} \quad \boldsymbol{G} = \underset{\boldsymbol{d}}{\operatorname{argmin}} \left\| \tilde{\boldsymbol{G}}'' - \boldsymbol{B}\boldsymbol{d} \right\|_2^2 \ . \tag{37}$$

The solution of both the minimum problems can be found by using the the Moore-Penrose pseudoinverse matrices, denoted as $\boldsymbol{A}^+, \boldsymbol{B}^+ \in \mathbb{R}^{N\times(M\cdot J)}$, respectively

$$\boldsymbol{G} = \boldsymbol{A}^+\tilde{\boldsymbol{G}}' \quad \text{or} \quad \boldsymbol{G} = \boldsymbol{B}^+\tilde{\boldsymbol{G}}'' \ . \tag{38}$$

It means that depending on the minimum problem solved, one can better approximate the elastic part or the loss part. Herein, by following the approach of Honerkamp [**honerkamp1989ill**], we build the two following matrices

$$\bar{\boldsymbol{G}} = \begin{bmatrix} \tilde{\boldsymbol{G}}' \\ \tilde{\boldsymbol{G}}'' \end{bmatrix} \in \mathbb{R}^{2(M\cdot J)\times 1} \quad \text{and} \quad \boldsymbol{C} = \begin{bmatrix} \boldsymbol{A} \\ \boldsymbol{B} \end{bmatrix} \in \mathbb{R}^{2(M\cdot J)\times N} \ . \tag{39}$$

The linear system to solve becomes

$$\boldsymbol{C}\boldsymbol{G} = \bar{\boldsymbol{G}} \ , \tag{40}$$

and the vector $\boldsymbol{G}$ can be obtained by solving the following minimum problem

$$\boldsymbol{G} = \underset{\boldsymbol{d}}{\operatorname{argmin}} \left\| \bar{\boldsymbol{G}} - \boldsymbol{C}\boldsymbol{d} \right\|_2^2 \ , \tag{41}$$

and therefore we could obtain $\boldsymbol{G}$ as the solution of the inverse problem

$$\boldsymbol{G} = \boldsymbol{C}^+\bar{\boldsymbol{G}} \ , \tag{42}$$

where $\boldsymbol{C}^+$ is the Moore-Penrose pseudoinverse matrix of $\boldsymbol{C}$. Since $\bar{\boldsymbol{G}}$ is a vector of experimental data, we can use the condition number, κ_0, as a measure of the magnification of the noise of the experimental data in the solution of the system of Equations 40 [**honerkamp1989determination**].

Obtaining the relaxation moduli using the Moore-Penrose pseudoinverse matrix could not be satisfactory [**honerkamp1989determination**]. In particular, $\boldsymbol{C}$ can be severely ill-conditioned: linear least-squares problems with a matrix of this kind are referred to as linear discrete ill-posed problem [**huang2016regularization**]. Calculating a meaningful solution of the relaxation moduli from the linear system of Equations 40 requires the system to be replaced by a nearby system that is less sensitive to perturbations, that is, a regularized system obtained by a regularization procedure [**calvetti2000tikhonov**].

The procedures that are typically implemented are the standard Tikhonov regularization procedure [**huang2016regularizatio**
(in detail in Tikhonov et al. [**tikhonov1995numerical**]) and the maximum entropy procedure [**bryan1990solving**].

In deriving the relaxation moduli from regularized systems, Honerkamp and Weese have shown that there are no substantial differences in the results using the two mentioned procedures [**honerkamp1989determination**]. For such a reason, we herein adopt the standard Tikhonov regularization procedure.

Using the standard Tikhonov regularization procedure means replacing the linear system of Equation 40 by the following regularized system [**calvetti2000tikhonov**]:

$$\left(\boldsymbol{C}^T\boldsymbol{C} + \mu\mathbf{1}\right)\boldsymbol{G} = \boldsymbol{C}^T\bar{\boldsymbol{G}} \ , \tag{43}$$

where $\mu \geq 0$ is the regularization parameter. For any fixed μ, the system has the unique solution

$$\boldsymbol{G}_\mu = \left(\boldsymbol{C}^T\boldsymbol{C} + \mu\mathbf{1}\right)^{-1}\boldsymbol{C}^T\bar{\boldsymbol{G}} \ , \tag{44}$$

where

- $\boldsymbol{G}_\mu = \underset{\boldsymbol{G}\in\mathbb{R}^N}{\operatorname{argmin}}\left\{ ||\boldsymbol{C}\boldsymbol{G} - \bar{\boldsymbol{G}}||_2^2 + \mu||\boldsymbol{G}||_2^2 \right\}$
- $\boldsymbol{G}_\mu \xrightarrow[\mu\to 0]{} \boldsymbol{G} = \boldsymbol{C}^+\bar{\boldsymbol{G}}$.

We choose the regularization parameter μ so that it minimizes the condition number κ_μ [**zhang2023new**], that is, the condition number of the matrix $\left(\boldsymbol{C}^T\boldsymbol{C} + \mu\mathbf{1}\right)^{-1}\boldsymbol{C}^T$. It is easy to note that $\kappa_\mu \to \kappa_0 = \kappa$ if $\mu \to 0$. In such a case, we are searching for a system that is as stable as possible under the perturbation of the experimental data $\bar{\boldsymbol{G}}$.

The proposed identification procedure has been tested on the benchmark dataset of Jalocha et al. [**jalocha2015revisiting**]. Results are shown in the Appendix.

It can be useful to have two measures of the error, one related to the elastic part and the other one related to the loss part. Therefore, we can introduce an elastic and a loss discrepancy, $\left\|\boldsymbol{d}_{G'}\right\|_2^2$ and $\left\|\boldsymbol{d}_{G''}\right\|_2^2$, respectively, as follows:

$$\left\|\boldsymbol{d}_{G'}\right\|_2^2 = \left\|\boldsymbol{A}\boldsymbol{G} - \tilde{\boldsymbol{G}}'\right\|_2^2 \quad \text{and} \quad \left\|\boldsymbol{d}_{G''}\right\|_2^2 = \left\|\boldsymbol{B}\boldsymbol{G} - \tilde{\boldsymbol{G}}''\right\|_2^2 \ . \tag{45}$$

We can measure the two errors $e_{G'}$ and $e_{G''}$ obtained by solving Equation 40 as follows:

$$e_{G'} = \frac{\left\|\boldsymbol{d}_{G'}\right\|_2^2}{\left\|\tilde{\boldsymbol{G}}'\right\|_2^2} \quad \text{and} \quad e_{G''} = \frac{\left\|\boldsymbol{d}_{G''}\right\|_2^2}{\left\|\tilde{\boldsymbol{G}}''\right\|_2^2} \ , \tag{46}$$

while, introducing the discrepancies of the regularized problem as

$$\left\|\boldsymbol{d}_{G'_\mu}\right\|_2^2 = \left\|\boldsymbol{A}\boldsymbol{G}_{\boldsymbol{\mu}} - \tilde{\boldsymbol{G}}'\right\|_2^2 \quad \text{and} \quad \left\|\boldsymbol{d}_{G''_\mu}\right\|_2^2 = \left\|\boldsymbol{B}\boldsymbol{G}_{\boldsymbol{\mu}} - \tilde{\boldsymbol{G}}''\right\|_2^2 \ , \tag{47}$$

we can obtain the two errors that we have solving the regularized problem of Equation 44 as

$$e_{G'_\mu} = \frac{\left\|\boldsymbol{d}_{G'_\mu}\right\|_2^2}{\left\|\tilde{\boldsymbol{G}}'\right\|_2^2} \quad \text{and} \quad e_{G''_\mu} = \frac{\left\|\boldsymbol{d}_{G''_\mu}\right\|_2^2}{\left\|\tilde{\boldsymbol{G}}''\right\|_2^2} \ . \tag{48}$$

To conclude, since by construction of the FTS mastercurves we have $\tilde{\boldsymbol{G}}' = \boldsymbol{G}'|_{T=T_{ref}}$ and $\tilde{\boldsymbol{G}}'' = \boldsymbol{G}''|_{T=T_{ref}}$, the obtained $\boldsymbol{G}$ (or even $\boldsymbol{G}_\mu$) is the vector of relaxation moduli at $T = T_{ref}$.

5. Results

Calorimetry. The results of our calorimetric analysis are shown in Figure 3(a) and (b). From Figure 3(a), we notice from the area of the highlighted peak that there is a considerable amount of semi-crystalline phase within the material, which also means that there is a consistent portion of the rigid amorphous phase. Figure 3(b) reports

that the glass transition related to the rigid amorphous phase starts at a temperature of about 50°C; however, before the transition is completed, the melting peak starts to develop (supporting the observation of Grebowicz et al. [**grebowicz1984thermal**]), because the slope of C_p of the melt phase (which is the slope of C_p right after the peak) is not yet reached when smaller crystals start to melt. The results agree with literature data on PP [**chen2022comprehensive**, **weingart2020comparison**].

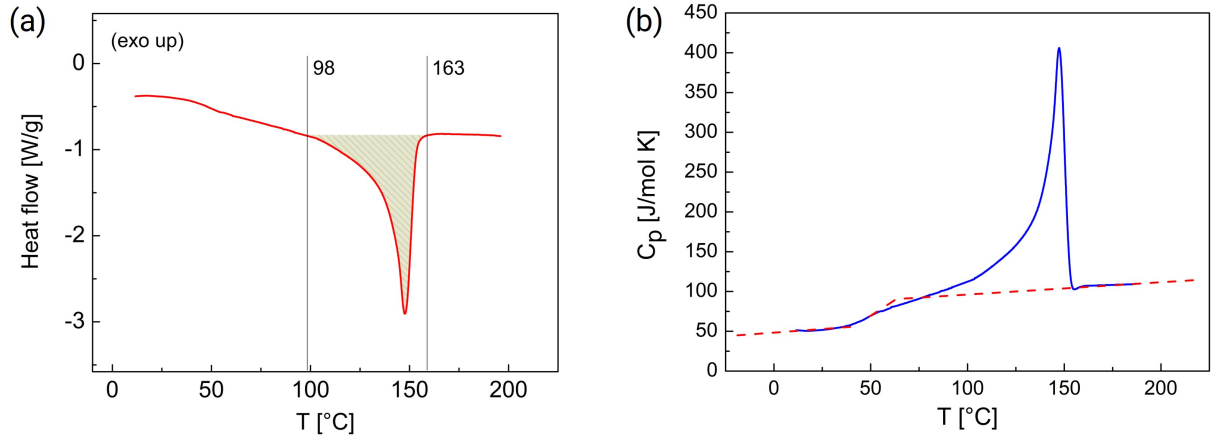

Figure 3: (a) PP heat flow curve versus temperature. The melting peak area is highlighted. (b) PP C_p versus temperature is reported with a blue line. The behavior of an ideal material with the two amorphous phases, but without crystals, is sketched with a dashed red line.

The concurrent change in microstructure during the glass transition of the rigid amorphous phase means that, to correctly predict the very low-frequency behavior of the material at reference temperature, one has to perform creep (or stress-relaxation) tests and then numerically move back to the frequency domain.

Dynamic mechanical analysis. We start by considering an isothermal shear frequency sweep test conducted with the DMA. From a single isothermal shear frequency sweep test, we obtain the storage modulus, G', and the loss modulus, G'', for any linear frequency $f = \omega/2\pi$ which belongs to the experimental window. A measure of the damping of the material as a function of the frequency is the *loss tangent*, $\tan\delta(f)$, defined as

$$\tan\delta(f) = \tan\left(\frac{G''(f)}{G'(f)}\right) \quad , \tag{49}$$

where $\delta(f) = G''(f)/G'(f)$ and it is often referred as loss angle [**anand2020continuum**].

We apply the FTS principle to a set of isothermal frequency sweep shear data (17 isothermal steps, ranging from -20°C to 120 °C), considering $T_{ref} = 30$ °C and according to the experimental procedure proposed by Arai and Ferry [**arai1986temperature**]. Such a procedure can be applied if: (i) we are in the linear viscoelastic regime and (ii) the $\tan\delta(f)$ has a nonzero curvature.

The procedure applies as follows: first, $\tan\delta(f)$ is shifted horizontally, that is, on the frequency axis. Second, we find the vertical shift function by vertically shifting the G' data. Automatically, the G'' data are correctly shifted with the same vertical shift function, due to condition (i). The result of the application of the shifting procedure (that is, the mastercurve) is shown in Figure 4. The error in such a shifting procedure can be estimated to be on the order of 5%, based on the results of Oseli et al. [**oseli2016time**].

Van Gurp and Palmen [**van1998time**] commented that TTS and FTS experimentally hold for a thermo-rheologically simple polymer when (i) the exact matching of shapes of consecutive (time- or frequency-dependent) curves is obtained, (ii) a_T is the same for all viscoelastic functions, and (iii) a_T has a reasonable physics-based functional form, such as the Arrhenius equation or the Williams-Landel-Ferry equation [**collyer1990polymer**, **tajvidi2005time**, **anand2020continuum**]. In our case, (i), (ii) and (iii) are fulfilled by adding the vertical shift

function b_T. It should be emphasized that in the nonlinear regime, the loss mechanisms are independent of the elastic mechanisms, and two different vertical shift functions would be needed for the storage and loss moduli [**fritzsche2010structural**].

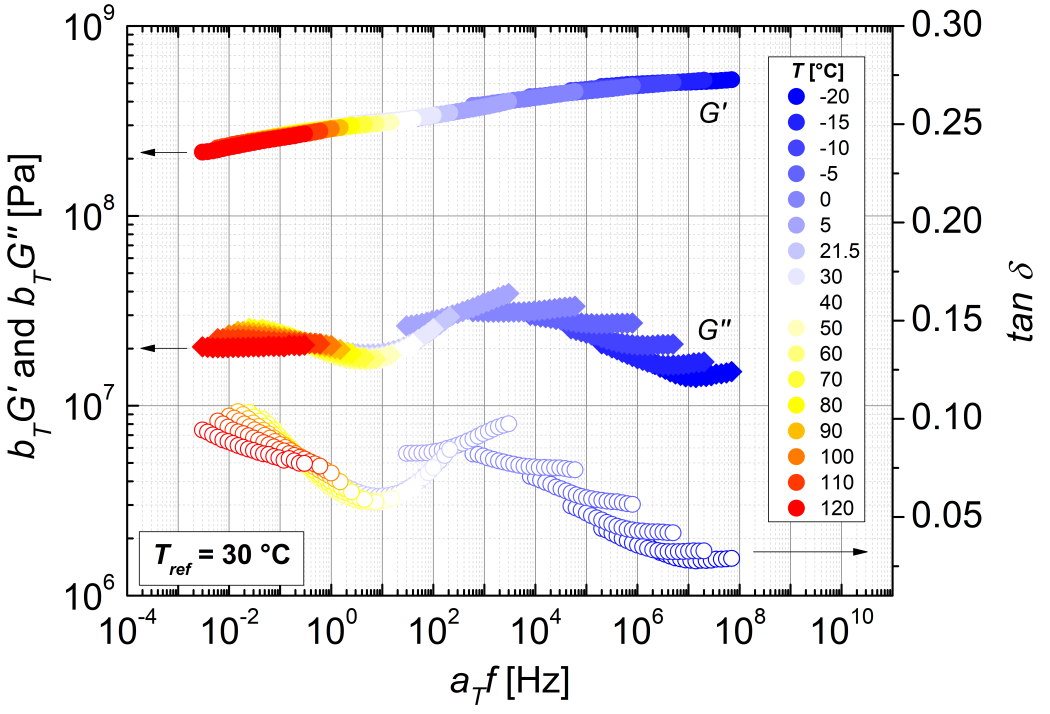

Figure 4: Application of the FTS principle on shear frequency sweep experimental data obtained at various temperatures, following the procedure proposed by Arai and Ferry [**arai1986temperature**].

In the mastercurve of Figure 4, two peaks in the tan δ function can be identified: the first around 10^3 Hz and related to the glass transition of the mobile amorphous phase; the second around 10^{-2} Hz and related to the glass transition of the rigid amorphous phase (which is, as espected from DSC results, not fully developed), while at high temperatures (roughly starting from 80 °C) the shifting procedure fails, even with the application of a vertical shift function, again according to the DSC results.

To confirm the failure of the FTS at high temperatures, we performed frequency sweep tests in tensile, shear and torsion setting with the temperature ranging from T_{ref} to 120 °C. Then, the FTS shifting procedure is applied and the resulting mastercurves, along with the Cole-Cole plots[5] and the Van Gurp and Palmen plots[6], are shown in Figures 5(a)-(i).

Viscoelastic functions are, in the range of the experimental error, independent of the geometry of the sample, the load condition, and the experimental setup. Moreover, all quantities are qualitatively and quantitatively coherent. The tan $\delta(f)$ of all types of loading is at least qualitatively the same, as also shown by Waterman [**waterman1977relations**]. This is a strong indication of the fact that the relaxation times in the linear viscoelastic regime are the same regardless of the load condition and that all the transitions seen reflect the material behavior and are not an artifact of the test.

[5] In the Cole-Cole plot, the loss moduli, G'', are plotted versus the loss moduli, G': isothermal frequency data combines into a mastercurve in the G'-G'' domain if the FTS holds [**friedrich1992generalized**].

[6] In their work in 1998, Van Gurp and Palmen plotted the phase angle, δ, of the rheological data versus the corresponding absolute value of the complex shear modulus, $|G^*|$, and found that isothermal frequency data combine into a mastercurve in the δ-$|G^*|$ domain if the FTS principle holds [**van1998time**].

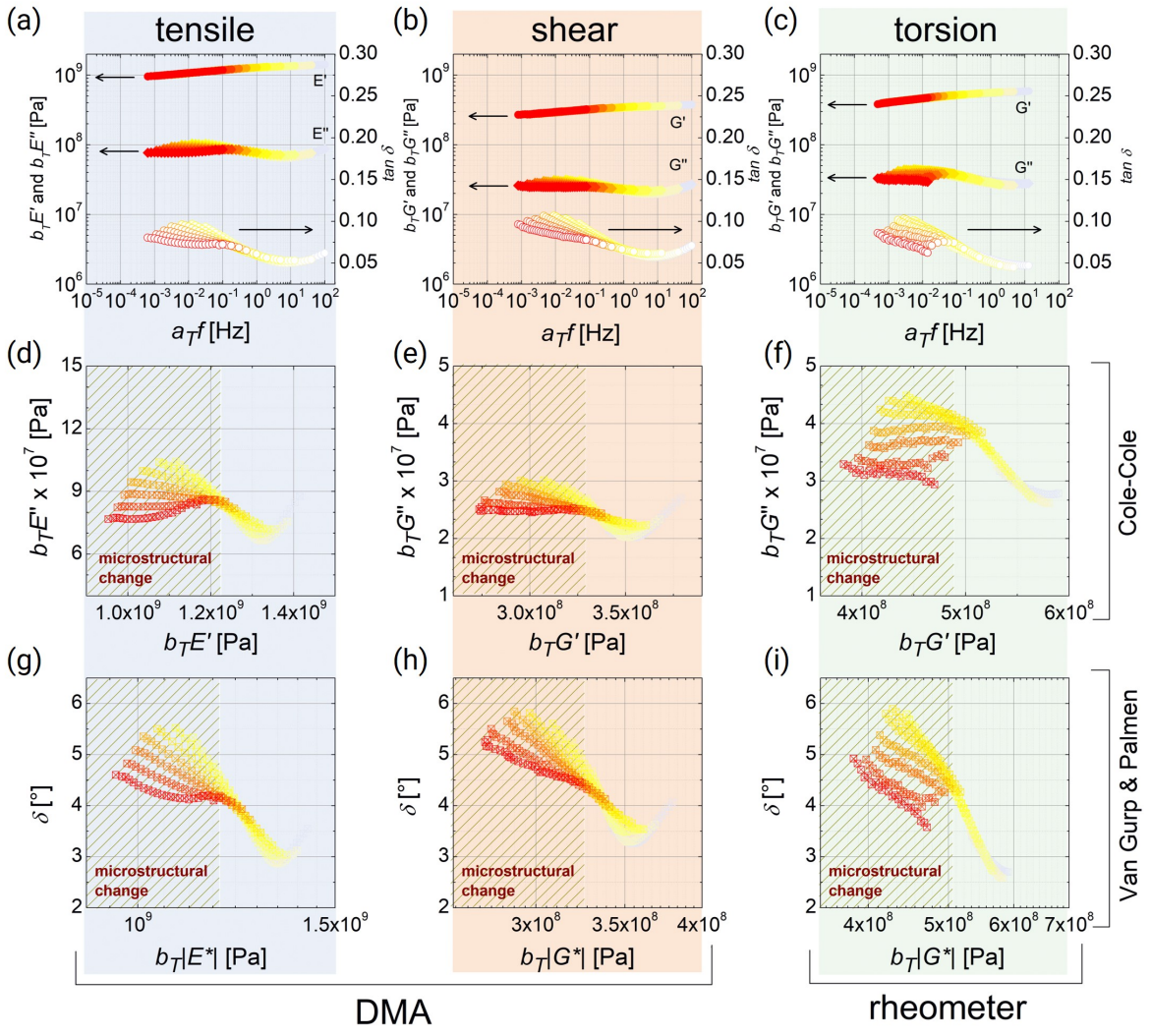

Figure 5: Column-wise: tensile, shear and torsion frequency sweep experiments on PP. Row-wise: FTS mastercurves, Cole-Cole plots and Van Gurp & Palmen plots. In all the tests, $T_{ref} = 30°C$. For the color legend, the reader can refer to Figure 4.

To further investigate the molecular nature of the phenomena involved, we can study the behavior of both a_T and b_T with temperature, reported in Figure 6(a) and (b) for all previous data sets. Different slopes highlights different structural transitions at the micro-scale.

To fit the experimental data, we adopt the Arrhenius equation, which reads [**collyer1990polymer**, **tajvidi2005time**]:

$$\ln a_T(T_n, T_{ref}) = \frac{E_{a_T}}{R}\left(\frac{1}{T_n} - \frac{1}{T_{ref}}\right) \quad \text{and} \quad \ln b_T(T_n, T_{ref}) = \frac{E_{b_T}}{R}\left(\frac{1}{T_n} - \frac{1}{T_{ref}}\right) , \tag{50}$$

where E_{a_T} and E_{b_T} are the fitting parameters, which represents the activation energies related to the horizontal and vertical shift functions, respectively, while R is the universal gas constant.

For E_{a_T}, we find $76^{\pm 2}$ kJ/mol (tensile), $79^{\pm 2}$ kJ/mol (shear), $88^{\pm 5}$ kJ/mol (torsion); while for E_{b_T} we found $19^{\pm 1}$ kJ/mol (tensile), $17^{\pm 1}$ kJ/mol (shear), $21^{\pm 1}$ kJ/mol (torsion). Hence, we find three coherent values of the activation energy, both for the horizontal and vertical shift functions.

Moreover, the temperature at which the change in slopes appears is the same for both functions, meaning that the vertical shift function can be linked to the effect on the moduli that a structural relaxation has, again as in the case of filled rubbers [**kluppel2008evaluation**, **fritzsche2010structural**, **garcia2023carbon**]. All results agree well with the results obtained by Collyer and Utracki [**collyer1990polymer**] for PP, who also applied the procedure proposed by Arai and Ferry [**arai1986temperature**] and the only difference is in the reference temperature choice, which was $T_{ref} = 50$ °C (see Appendix for details).

The overall experimental framework (DSC and DMA data) tells us that the vertical shift function trend can be interpreted again considering various structural transitions at the micro-scale. Indeed, recently, the introduction of the vertical shift function in FTS mastercurves has been investigated for filler-reinforced elastomers [**kluppel2008evaluation**, **fritzsche2010structural**, **garcia2023carbon**], and should be also emphasized that due to physical analogies, filled rubbers and semi-crystalline polymers can be dealt with using a common approach [**struik1978physical**]. Recalling the Introduction, in the case of semi-crystalline polymers, the crystals act as a filler and broaden the glass transition due to the rigid amorphous phase, that is, due to constrained chains and tie molecules between crystals [**struik1987mechanical**], in a way similar to that of filled rubbers. In such a situation, we could suppose that the vertical shift function will be related to changes in the mobility of constrained macromolecules in the presence of crystals or solid particles [**collyer1990polymer**], and such a statement is supported by our calorimetry data.

What we can observe from the DMA experimental investigation is that when the temperature is below the glass transition temperature of the mobile amorphous phase, b_T is roughly constant and there is almost no direct effect of the temperature on the viscoelastic functions. However, when the temperature overcomes the glass transition of the mobile amorphous phase, the macro-mechanics is governed by the behavior of the rigid amorphous phase between the crystals (such a mobile amorphous phase has a higher, and broader, glass transition temperature, as can be seen in Figure 3(a) and (b)): b_T changes its slope and seems to be well described by an Arrhenius equation. Before such a broad transition is completed, small crystals start to melt, and the slope of b_T changes again, possibly combining multiple effects at the micro-scale.

From the experimental data we can conclude that b_T, while mathematically describes the additional temperature dependence of the viscoelastic functions, it turns out that it could be physically linked to thermally activated mechanisms that directly affect the stiffness of the material (in the case of semi-crystalline polymers, such a mechanisms could affect the much stiff constrained molecules between crystals).

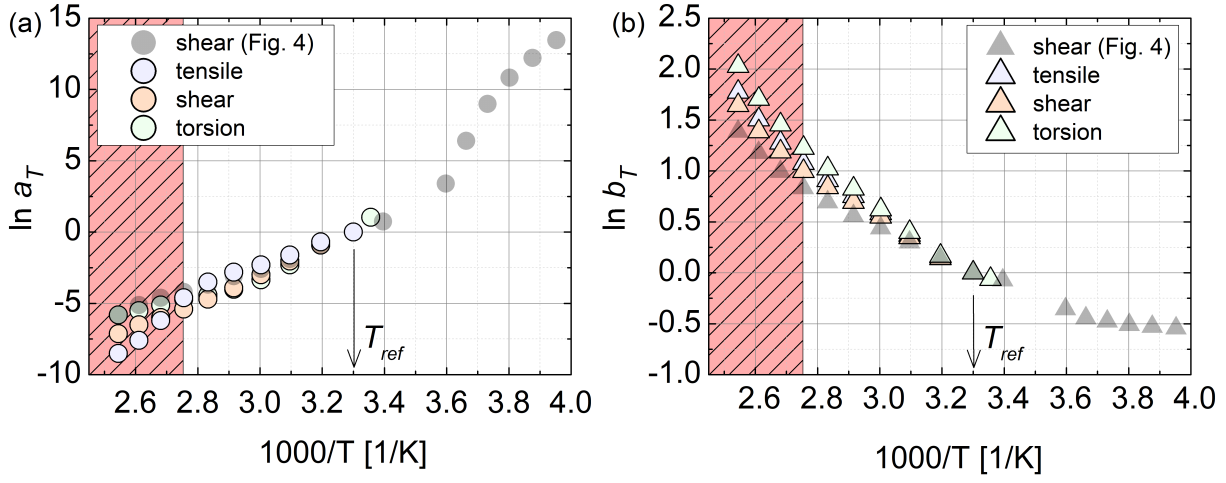

Figure 6: Shift function values versus $1000/T$. In transparency, we report the shift function values of Figure 4 for proper comparison. The red area represent the area in which the microstructure is changing.(a) Horizontal shift function (a_T). (b) Vertical shift function (b_T).

Identification. We should note that from Figure 5 that it is not possible to predict the behavior of the material at very low frequencies from the mastercurves, since the change in microstructure due to melting (as supported by

Figure 3) does not allow such a prediction. Hence, only for the identification step we set $G_\infty = 0$ to avoid artifacts, similar to the approach taken by Jalocha et al. [**jalocha2015revisiting**].

Once the rheological model for the identification procedure is defined, the aim of the identification procedure is to identify (i) the number N and the values of the relaxation times at the reference temperature, $\tau_j|_{T_{ref}}$ and (ii) the values of the corresponding relaxation moduli at the reference temperature, $G_j|_{T_{ref}}$. Once $\tau_j|_{T_{ref}}$ and $G_j|_{T_{ref}}$ are obtained, we can predict the behavior of the material in the time domain under isothermal conditions, specifically at $T = T_{ref}$.

The results of the application of *Step 1* and *Step 2* are shown in Figures 7(a) and (b) respectively (while the values of the relaxation times and the respective relaxation moduli are reported in the Table A.3 of the Appendix).

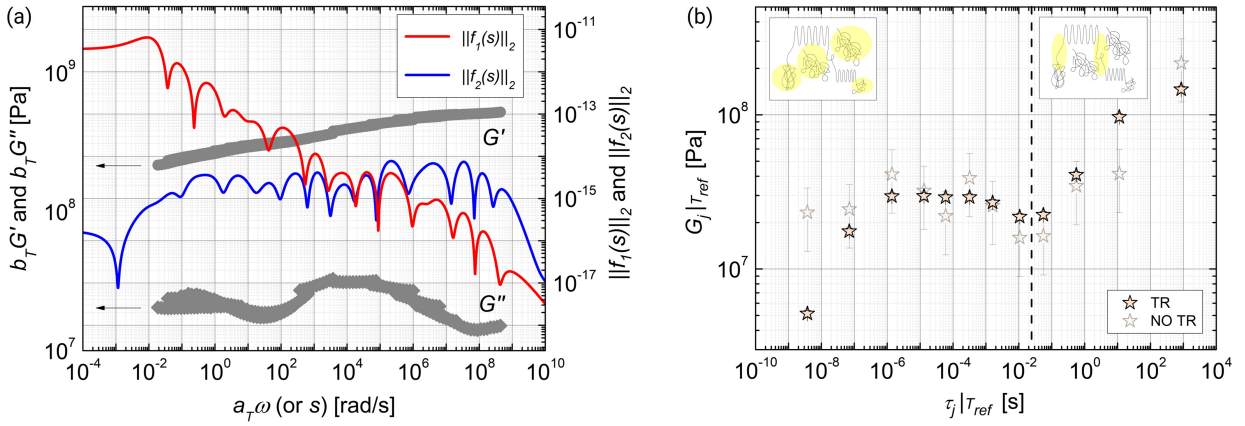

Figure 7: (a) Result of *Step 1*. On the left axis, we report the FTS mastercurves for the storage and loss moduli shown in Figure 4 versus the shifted angular frequency. On the right axis, we show the functions $||f_1(s)||_2$ and $||f_2(s)||_2$ as a function of s (which here corresponds numerically to the angular frequency). (b) Result of *Step 2*. We report the values of $G_j|_{T_{ref}}$ versus the correspondent relaxation times $\tau_j|_{T_{ref}}$ along with the estimated error bars both with and without the application of the Tikhonov regularization procedure (TR and NO TR, respectively). In the upper insets, a schematic of the micro-scale where the region of interest for the transitions are highlighted.

From Figure 7(a), we can observe the zeros (in a numerical sense) of both $||f_1(s)||_2$ and $||f_2(s)||_2$, as similarly obtained by Jalocha et al. [**jalocha2015revisiting**]. Since we have built the functions using a mastercurve obtained by shifting the curves with respect to a reference temperature T_{ref}, the common zeros of the functions correspond to the reciprocal relaxation times at the reference temperature, $\tau_j|_{T_{ref}}$. To obtain a precise numerical correspondence between the zeros of the two functions, a regularization procedure should be used even for the present step [**jalocha2015revisiting**, **hansen1992numerical**, **honerkamp1989ill**]. However, it has been shown that using regularization with the proposed identification method, some relaxation times can be lost [**jalocha2015revisiting**]. For such a reason, we take as relaxation times the zeros of the function $||f_2(s)||_2$, since it also predicts an asymptotic relaxation time and it is of importance for a correct calculation of the relaxation moduli [**honerkamp1989ill**].

In Figure 7(b), we show the values of $G_j|_{T_{ref}}$ versus the correspondent relaxation times $\tau_j|_{T_{ref}}$, both with and without the application of the Tikhonov regularization procedure. We have estimated the errors in the calculated moduli by multiplying the moduli values by the experimental error on the measurement (1.5%) and by the condition number of the matrix $\left(\boldsymbol{C}^T\boldsymbol{C} + \mu\mathbf{1}\right)^{-1}\boldsymbol{C}^T$ (when the Tikhonov regularization is applied, TR) or of the matrix $\boldsymbol{C}$ (when the Tikhonov regularization is not applied, NO TR). As can be noticed, the Tikhonov regularization reduces the oscillation stabilizing the solution, and a more clear trend can be observed.

Based on dynamic mechanical and calorimetric results, two sets of relaxation moduli can be identified. Below a characteristic time of $\sim 10^{-1}$ s, we can find the relaxation times and moduli connected to the behavior of the mobile amorphous phase, since such a phase is not microscopically constrained by the surrounding crystals, resulting in a faster macroscopic mechanical relaxation (schematic in the left-inset of Figure 7(b)). Above a characteristic time of $\sim 10^{-1}$, we can find the relaxation times and moduli related to the rigid amorphous phase (which is present and in a non-negligible amount, as shown by calorimetry results) can only relax at longer times due to the constraints of the macromolecules at the microscale (schematic in the right-inset of Figure 7(b)).

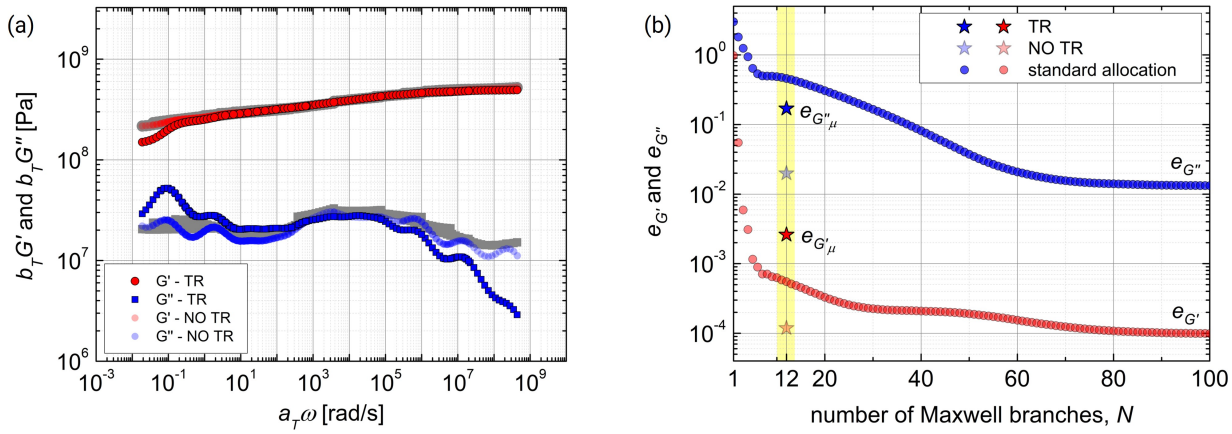

Figure 8: (c) Model prediction (Equation 24) using the parameter obtained by the identification procedure, with (TR) and without (NO TR) the Tikhonov regularization step. (d) Error on the elastic and loss part.

In Figure 8(c) we report the behavior of the model compared to the original data set. In Figure 8(d) we report the errors of the elastic and loss part given by the application of Step 2 after Step 1 with and without the Tickhonov regularization step (full and transparent stars), compared with the application of Step 2 after a standard allocation of relaxation times.

Validation. To validate the model, the numerical simulations of stress-relaxation and creep tests are performed under the same conditions as the experiments. Numerically, (i) the stress-relaxation experiment is a mixed-controlled problem, where we impose $\epsilon_1 = \epsilon_0$ and $\sigma_2 = \sigma_3 = \sigma_{23} = \sigma_{13} = \sigma_{12} = 0$ and we compute the uniaxial tensile stress-relaxation function as $E_1(t) = \sigma_1(t)/\epsilon_0$, while (ii) the creep test is entirely force controlled, where we apply $\sigma_1 = \sigma_0$ and $\sigma_2 = \sigma_3 = \sigma_{23} = \sigma_{13} = \sigma_{12} = 0$ and we compute the numerical uniaxial tensile creep compliance as $J_1(t) = \epsilon_1(t)/\sigma_0$.

As widely assumed in the literature, we assume a purely elastic volumetric response and therefore that the bulk relaxation is negligible [**tschoegl2002poisson**, **anand2020continuum**, **lenarda2022computational**, **dusane2023computational**] From the assumption of isotropy, it is reasonable to assume

$$K|_{T_{ref}} = \frac{2G_0|_{T_{ref}}(1+\nu)}{3(1-2\nu)} \ , \tag{51}$$

where $G_0|_{T_{ref}} = G_\infty + \sum_j^N G_j|_{T_{ref}}$ and it represents the glassy shear modulus of the material. The value of the Poisson ratio can be found in the literature for PP, and it is assumed $\nu = 0.41$ [**tscharnuter2011time**]. The only parameter that must be tuned is G_∞, which cannot be obtained from our mastercurves, and we choose the value of $G_\infty = 1.6 \times 10^8$ Pa so that the experimental tensile creep compliance coincides with the simulated one. With this value of G_∞, we obtain $K|_{T_{ref}} = 3.4 \times 10^9$ Pa, which is consistent with literature results [**andersson1997thermal**, **gluge2019effective**].

It should be emphasized that if the hypotheses of the model are valid, from the identification procedure we have obtained the relaxation times and moduli at T_{ref}. Hence, we can simulate the behavior of the polymer in the time-domain at $T = T_{ref}$: that is why stress-relaxation and creep tests are carried out at $T = T_{ref}$, such that the experimental and numerical curves can be directly compared without any other assumption.

Comparisons between the model and the experimental results in the time domain are reported in Figures 9(a) and (b). From both 9(a) and 9(b), we can notice that the model shows reasonable agreement with the slope of $J_1(t)$ and $E_1(t)$ at short times and long times and the main slope change at ~ 200 s, and therefore seems to successfully capture the physics of the underlying structural transitions with the simple addition of the vertical shift function. At ~ 20 s, a larger deviation is observed. This can be eventually managed by increasing the number of relaxation times, but this will increase the computational cost and, moreover, the values of such added relaxation times would be arbitrary.

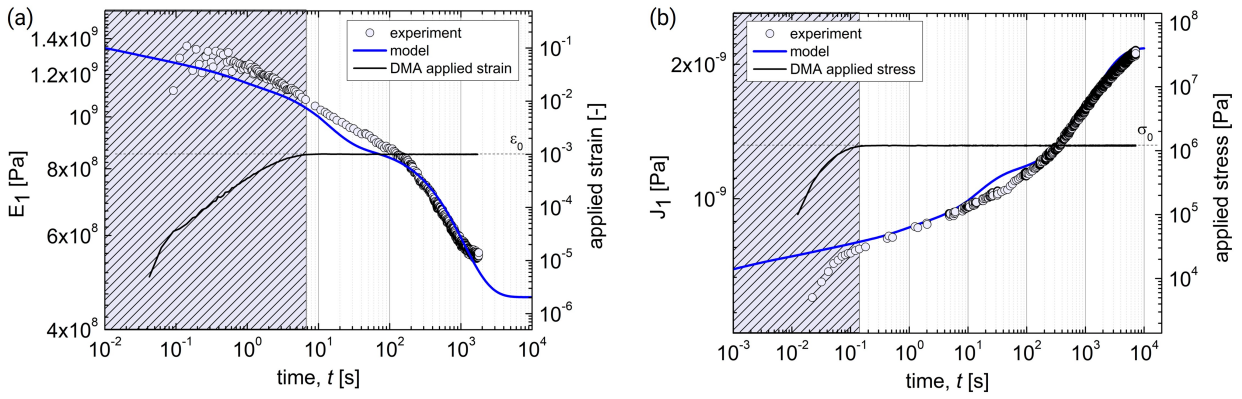

Figure 9: Experimental validation in the time-domain of the model with parameters obtained in the frequency domain. The highlighted regions are regions in which the measure is not reliable due to DMA hardware constraints (i.e., transient in the application of stress/strain). (a) Uniaxial tensile stress-relaxation test. (b) Uniaxial tensile creep test.

Prediction. Once the procedure has been validated at $T_{ref} = 30$ °C and since a_T and b_T are known for a given subset of temperatures, by Equation 24 we can predict the behavior of the PP in the frequency domain at different reference temperatures. In Figure 10(a) we show the predicted behavior of the storage modulus of the material by taking as the reference temperature all the temperatures experimentally explored to build the mastercurve of Figure 4. In Figure 10(b) we report the corresponding relxation moduli.

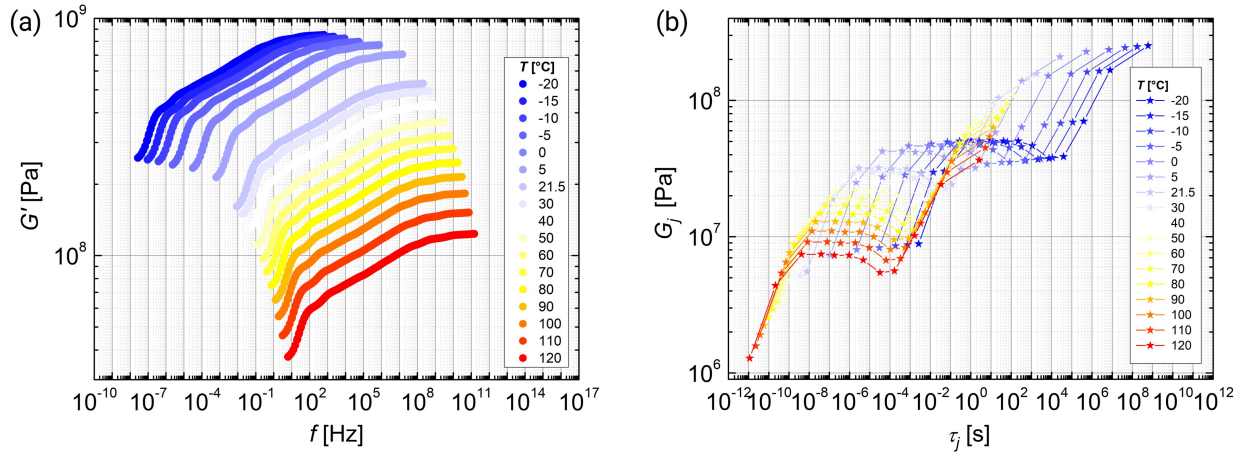

Figure 10: (a) Prediction of the storage moduli mastercurves at different reference temperatures. The data of Figure 4 are also reported for proper comparison, and the experimental window is highlighted. (b) Prediction of relaxation moduli at different temperatures.

From Figure 10(a), it can be noticed that, with respect to the curve with a reference temperature of 30 °C, if the reference temperature is lower, the storage modulus is higher (the effect of b_T) and the behavior of the material can be obtained up to $\omega = 10^{-7}$ rad/s (the effect of a_T); on the contrary, if the reference temperature is higher than 30 °C, the storage modulus is lower (the effect of b_T) and the behavior can be obtained in the very high frequency range, even above $\omega = 10^{10}$ rad/s (the effect of a_T). Accordingly, as shown in Figure 10(b), in relation to the curve with a reference temperature of 30 °C, a lower reference temperature results in higher relaxation moduli and relaxation times, owing to the slower rearrangement of macromolecules and the maintained stiffness of the network between crystals. In contrast, at a higher reference temperature, both relaxation moduli and times decrease, as macromolecules rearrange

more easily and the network between crystals becomes less stiff.

Applicability and limitations of the model. The model is applicable only if the microstructure remains unchanged under the testing conditions. When dealing with semi-crystalline polymers, the microstructure can evolve with temperature. In the particular case investigated, experiments show that around 100°C, the microstructure changes due to the evolution and modification of the crystals, thereby completely altering the macroscopic mechanical behavior of the thermo-rheologically complex polymer. The proposed approach relies on the fact that it is primarily the amorphous (rigid or mobile) phase that governs the mechanics of such systems when (i) strain is sufficiently small and (ii) temperature does not alter the microstructure through crystal evolution. The amorphous phase allows, with varying efficiency, for load transfer between the crystals. As the temperature increases, the network between the crystals becomes weaker (an effect accounted for in b_T), and the load-carrying capability of the thermo-rheologically complex polymer decreases, which is considered in the model; however, an excessively high temperature will induce changes in the microstructure, and the model will no longer be valid. Additionally, the model is developed within the framework of linear viscoelasticity. If the strain exceeds a threshold of approximately 1%, the crystals begin to align in the direction of loading, again altering the microstructure (from the perspective of filler orientation) and impacting the mechanical behavior of the system [**dong2014dependence**]; such an effect strongly influences the relaxation moduli and is not captured by the proposed model.

6. Conclusion

In this work, we have proposed a simple multiaxial constitutive model for the linear viscoelastic behavior of thermo-rheologically complex polymers. Inspired by the work of Harper and Weitsman [**harper1985characterization**], such a model includes both the horizontal and vertical shift functions that can be found experimentally with classical experimental methods (i.e., DMA), both in the time and frequency domain. We have described the numerical implementation and the parameter identification procedure, based on the work of Jalocha et al. [**jalocha2015revisiting**] in which we have implemented a regularization step to face the ill-posed identification problem. We have performed calorimetry analysis and tensile, shear and torsion frequency sweep experiments on PP (a semi-crystalline polymer, hence thermo-rheologically complex) to search for the horizontal and vertical shift functions, obtained through the application of the FTS procedure (following Arai and Ferry [**arai1986temperature**]) and we have found coherence between the experimental approaches and the literature. We have calibrated our model on the FTS shear mastercurve and validated it in the time domain, by means of stress-relaxation and creep experiments. In conclusion, we have shown some model predictions for different temperatures, and we have discussed its limitations. This work could serve as a foundation for the development of nonlinear, physics-based continuum mechanical models for thermo-rheologically complex polymers, with the final goal of having a powerful tool to predict the macroscopic mechanical behavior of a thermo-rheologically complex polymer in both the time and frequency domains.

A. Appendix

Fourth-order tensors and notation. We start considering two second-order tensors, $\boldsymbol{A}$ and $\boldsymbol{B}$, with $\boldsymbol{A}^T$ and $\boldsymbol{B}^T$ their transpose, respectively. Following Kellerman et al. [**kellermann2021fourth**], we can define the three fundamentals operations indicially, in an orthonormal basis, as

$$[\boldsymbol{A} \otimes \boldsymbol{B}]_{ijkl} = A_{ij}B_{kl}, \quad [\boldsymbol{A} \odot \boldsymbol{B}]_{ijkl} = A_{ik}B_{lj}, \quad \text{and} \quad [\boldsymbol{A} \circledast \boldsymbol{B}]_{ijkl} = A_{il}B_{jk} \ . \tag{52}$$

Starting by the second-order identity tensor, $\mathbf{1}$, the three proposed operators, lead to three fourth-order tensors [**kellermann2021fourth**]:

$$\underset{\otimes}{\mathbb{I}} = \mathbf{1} \otimes \mathbf{1}, \quad \underset{\odot}{\mathbb{I}} = \mathbf{1} \odot \mathbf{1}, \quad \text{and} \quad \underset{\circledast}{\mathbb{I}} = \mathbf{1} \circledast \mathbf{1} \ . \tag{53}$$

Following Itskov [**itskov2007tensor**], We can define the super-symmetric identity tensor as:

$$\underset{\odot}{\mathbb{I}}^{\mathrm{Ss}} = \frac{1}{2}\left(\underset{\odot}{\mathbb{I}} + \underset{\circledast}{\mathbb{I}}\right) \ , \tag{54}$$

which maps any arbitrary (non necessarily symmetric) second order tensor into its symmetric part [**itskov2007tensor**]. We can also define the super-symmetric fourth-order deviatoric projection tensor as:

$$\underset{\odot_{\text{dev}}}{\mathbb{I}}^{\text{Ss}} = \underset{\odot}{\mathbb{I}}^{\text{Ss}} - \frac{1}{3}\mathbb{I}\otimes\mathbb{I} \ . \tag{55}$$

Properties of the Laplace transform. We can define the Laplace transform of the function $f(t) : [0, \infty) \to \mathbb{R}$ as

$$\mathscr{L}[f(t)] = \int_{0^-}^{\infty} e^{-st} f(t) \mathrm{d}t \ , \tag{56}$$

where $s = a + \mathrm{i}\omega \in \mathbb{C}$ is the complex variable. The Laplace transform has some important properties of interest for the present work, which are:

1. $\mathscr{L}[bf(t) + cg(t)](s) = b\mathscr{L}[f(t)](s) + c\mathscr{L}[g(t)](s) \quad \text{with } b, c \in \mathbb{R}$
2. $\mathscr{L}[\dot{f}(t)] = s\mathscr{L}[f(t)](s) - f(0^-)$
3. $\mathscr{L}[1](s) = \dfrac{1}{s}$
4. $\mathscr{L}[\exp(dt)](s) = \dfrac{1}{s-d} \text{ with } d \in \mathbb{R} \ .$

If we consider two time dependent functions, $f(t)$ and $g(t)$, the convolution between the two functions, $(f * g)(t)$, is defined as

$$(f * g)(t) \overset{\text{def}}{=} \int_{-\infty}^{\infty} f(t-\tau) g(\tau) \mathrm{d}\tau \ , \tag{57}$$

the convolution is commutative and if $f(t), g(t) : [0, \infty) \to \mathbb{R}$, the integration limit can be truncated such that

$$(f * g)(t) \overset{\text{def}}{=} \int_{0}^{\infty} f(t-\tau) g(\tau) \mathrm{d}\tau \ . \tag{58}$$

The Laplace transform of such a convolution is

$$\mathscr{L}[(f * g)(t)] = \mathscr{L}[f(t)]\mathscr{L}[g(t)] \ . \tag{59}$$

which is of particular importance in deriving viscoelastic models in the frequency domain starting from the time domain.

Numerical implementation with flattening operators. Due to the symmetry of the tensors involved in the model development, we can introduce the Voigt half-vectorization map [**kellermann2021fourth**]:

$$\mathbf{V} : (x, y) \in (\{1, ..., n\}, \{1, ..., n\}) \to z \in \{1, ..., S(n)\} \ , \tag{60}$$

that is, as an operator that turn a $n \times n$ symmetric tensor $\boldsymbol{A}$ into a $S(n) \times 1$ array vector, $\{\boldsymbol{A}\}$, where $S(n)$ is the Gauss sum of n.[7] In the definition (x, y) are the tensor indices, while z is the vector index. For the case of symmetric 3×3 tensors, the form of the map is the following:

$$V_{xy} = z \quad \text{such that} \quad \mathbf{V} = \begin{bmatrix} V_{11} & V_{12} & V_{13} \\ \cdot & V_{22} & V_{23} \\ \cdot & \cdot & V_{33} \end{bmatrix} = \begin{bmatrix} 1 & 6 & 5 \\ \cdot & 2 & 4 \\ \cdot & \cdot & 3 \end{bmatrix} \ , \tag{61}$$

where, due to the symmetry, the elements at positions $(\cdot)$ will not be included in the final 6×1 vector. In other words, $\mathbf{V}$ serves as a mapping between tensor indices and matrix array positions. Specifically, given the $n \times n$ tensor indices

[7] The Gauss sum applied to n gives the sum of the firs n natural numbers, i.e., $S(n) = n\dfrac{(n+1)}{2}$.

Relaxation times	τ_1 [s]	τ_2 [s]	τ_3 [s]	τ_4 [s]
Benchmark [**jalocha2015revisiting**]	0.05	0.2	2	10
Obtained from $\|\|f_1(s)\|\|_2$	0.050	0.25	1.9	7.1
Obtained from $\|\|f_2(s)\|\|_2$	0.034	0.18	2.1	12.6

Table A.1
Step 1: identification of relaxation times. Comparison between the benchmark data of Jalocha et al. and values predicted by the identification procedure [**jalocha2015revisiting**].

(x, y) as input, the value z at the corresponding position in $\mathbf{V}$ represents the vector index, ranging from 1 to $S(n)$, as output.

The outcome of the half-vectorization map applied to the symmetric tensor $\boldsymbol{A}$ is the vector called *half-vectorized tensor* $\{\boldsymbol{A}\}$ (with components $\{\boldsymbol{A}\}_z$), that is

$$\{\boldsymbol{A}\}_z = \{\boldsymbol{A}\}_{V_{xy}} = A_{xy} \ , \tag{62}$$

and therefore

$$\{\boldsymbol{A}\}^T = \begin{bmatrix} A_{11} & A_{22} & A_{33} & A_{23} & A_{13} & A_{12} \end{bmatrix}^T \ . \tag{63}$$

The half-vectorized vectors $\{\mathbf{1}\}$, $\{\boldsymbol{\sigma}\}$ and $\{\boldsymbol{\epsilon}\}$ of the tensors $\mathbf{1}$, $\boldsymbol{\sigma}$ and $\boldsymbol{\epsilon}$, respectively, are

$$\begin{aligned} \{\mathbf{1}\} &= \begin{bmatrix} 1 & 1 & 1 & 0 & 0 & 0 \end{bmatrix}^T \\ \{\boldsymbol{\sigma}\} &= \begin{bmatrix} \sigma_{11} & \sigma_{22} & \sigma_{33} & \sigma_{23} & \sigma_{13} & \sigma_{12} \end{bmatrix}^T \\ \{\boldsymbol{\epsilon}\} &= \begin{bmatrix} \epsilon_{11} & \epsilon_{22} & \epsilon_{33} & \epsilon_{23} & \epsilon_{13} & \epsilon_{12} \end{bmatrix}^T \ . \end{aligned} \tag{64}$$

In a consistent way, we can define a flattening operator that can *unfold* a fourth-order tensor of dimensions $n \times n \times n \times n$ in a matrix of dimensions $S(n) \times S(n)$. Coherently with the above defined half-vectorization map, we can define the fourth-order tensor-to-matrix flattening operator $[\cdot]^{\odot}$ that acts on the tensor $\mathbb{A}$ such that

$$A_{ijkl} = [\mathbb{A}]^{\odot}_{V_{ij}V_{kl}} = [\mathbb{A}]^{\odot}_{z_1 z_2} \ . \tag{65}$$

We use the symbol $[\cdot]^{\odot}$ since it is the same symbol used by Kellermann et al. for such an operation [**kellermann2021fourth**], and the reader can easily get more information and properties in the original work of the authors. In such a framework, the flattened tangent matrix, $\left[\mathbb{C}_{\mathrm{TG}}\right]^{\odot}$, for the Newton-Rapson algorithm becomes:

$$\left[\mathbb{C}_{\mathrm{TG}}\right]^{\odot} = b_{T_n}\left(K_\infty + \sum_j K_j \alpha_j\right)\left[\mathbb{I}_{\otimes}\right]^{\odot} + 2b_{T_n}\left(G_\infty + \sum_j G_j \alpha_j\right)\left[\mathbb{I}^{\mathrm{Ss}}_{\odot\mathrm{dev}}\right]^{\odot} \ . \tag{66}$$

Validation of the identification code. Our identification method has been specifically modified to match the identification code proposed by Jalocha et al. [**jalocha2015revisiting**] for proper check on their benchmark problem by using the data available in their work. specifically, the particular case proposed by Jalocha et al. [**jalocha2015revisiting**] is obtained by imposing $a_T = b_T = 1$ and $\mu = 0$. The results are shown in Figure A.1, while the values of relaxation times and relaxation moduli are shown in Table A.1 and Table A.2, respectively. As can be seen, the method is capable of identifying (within a certain error), all the relaxation times and moduli, even overcoming the problem of the highest relaxation time encountered by Jalocha et al. [**jalocha2015revisiting**].

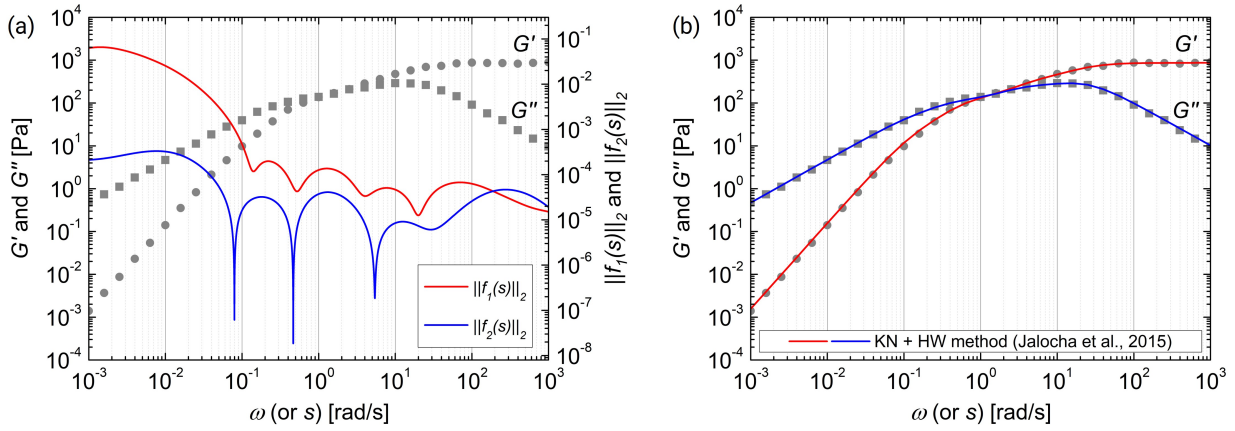

Figure A.1: Identification step applied on the benchmark problem of Jalocha et al. [**jalocha2015revisiting**].

Relaxation moduli	G_1 [Pa]	G_2 [Pa]	G_3 [Pa]	G_4 [Pa]
Benchmark [**jalocha2015revisiting**]	400	300	150	8
Obtained with τ_j from $\|\|f_1(s)\|\|_2$ and $\boldsymbol{A}^+$	453.9	271.1	119	22.1
Obtained with τ from $\|\|f_1(s)\|\|_2$ and $\boldsymbol{B}^+$	439.17	275.2	130.6	19.7

Table A.2
Step 2: identification of relaxation moduli. Comparison between the benchmark data of Jalocha et al. and values predicted by the identification procedure [**jalocha2015revisiting**].

Validation of the experimental data. In Figures A.2(a) and (b) we report the comparison of our experimental data with the one obtained by Collyer and Utracki [**collyer1990polymer**], in terms of mastercurves and shift factors, respectively. In particular, the data are reported as in the original work of the authors, without performing any

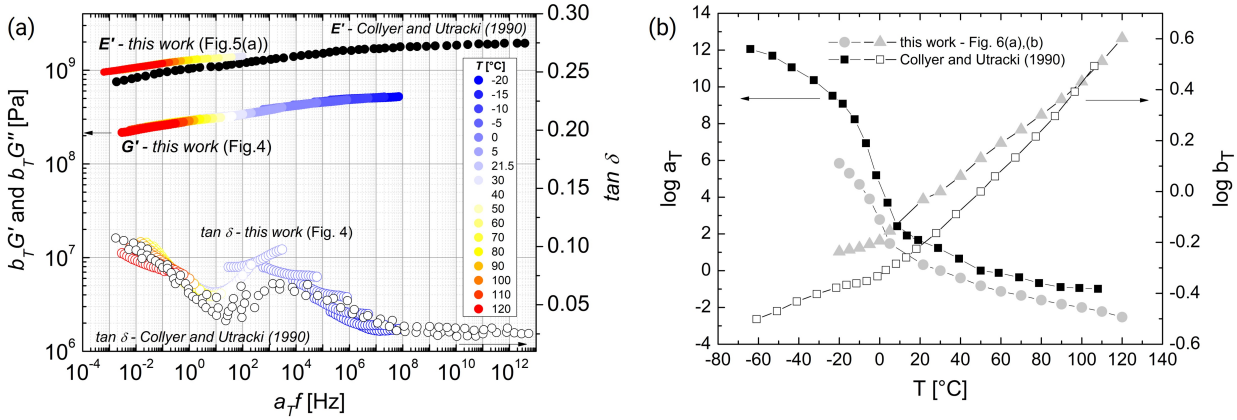

Figure A.2: Comparison with the work of Collyer and Utracki [**collyer1990polymer**]. We emphasize that Collyer and Utracki used $T_{ref} = 50$ °C [**collyer1990polymer**]. (a) Mastercurves. (b) Shift functions.

supplementary computation. The different experimental window and (ii) the choice of the reference temperature: (i) should not influence the result, since the tan δ curve of the PP is highly nonmonotonic, and it is easy to get the values of a_T (and hence b_T) by the Arai and Ferry procedure [**arai1986temperature**]; from (ii) we can understand that there should be a difference of only a vertical constant between the horizontal and vertical shift functions obtained in this

Identification procedure result												
j-branch	1	2	3	4	5	6	7	8	9	10	11	12
$\log \tau_j$ [s]	6.76	2.42	-0.59	-2.89	-4.54	-6.44	-8.05	-9.72	-11.24	-13.48	-16.47	-19.4
$G_j\|_{T_{ref}}$ [MPa] NO TR	215.8	41.4	34.6	16.3	16.0	25.7	38.9	22.0	32.2	41.1	24.4	23.3
$G_j\|_{T_{ref}}$ [MPa] TR	146.1	96.8	40.8	22.4	21.8	26.9	29.2	29.2	29.7	29.6	17.5	5.1

Table A.3
Identification procedure result. τ_j values are obtained from *Step 1*, while $G_j|_{T_{ref}}$ values from *Step 2* with and without the Tikhonov regularization procedure (TR and NO TR, respectively).

work and those obtained by Collyer and Utracki [**collyer1990polymer**]. We emphasize that also in the work of Collyer and Utracki the b_T is unique for the storage and loss moduli, since (as done by us in this work) they carried out the experiments in the linear regime and the Kramers-Koning relationship must be fulfilled [**fritzsche2010structural**]. Looking at Figure A.2(a), in the case of Collyer and Utracki we can notice that their $\tan\delta$ curve is shifted to higher frequencies and that their E' mastercurve is shifted to lower values. This is expected since they used $T_{ref} = 50$ °C, and this is in agreement with the predictions of Figure 10(a).

Values obtained from the identification step. We report in Table A.3 the relaxation times and moduli obtained from the application of the identification procedure.

B. Data availability statement

Experimental data and numerical codes (implemented in MATLAB®) are available at https://github.com/paolo-iaccarino/thermo-rheo_complex.

C. Acknowledgments

This research received no specific grant from any funding agency in the public, commercial, or not-for-profit sectors.

D. Declaration of competing interest

The authors declare that they have no known competing financial interests or personal relationships that could have appeared to influence the work reported in this paper.

CRediT authorship contribution statement

Paolo Iaccarino: conceptualization, methodology, software, validation, formal analysis, investigation, data curation, writing (original & review and editing), visualization. **Ernesto Di Maio:** resources, writing (review and editing), visualization, supervision. **Andrei Constantinescu:** conceptualization, methodology, writing (review and editing), visualization, supervision. **Ferdinando Auricchio:** conceptualization, methodology, resources, writing (review and editing), visualization, supervision, project administration.